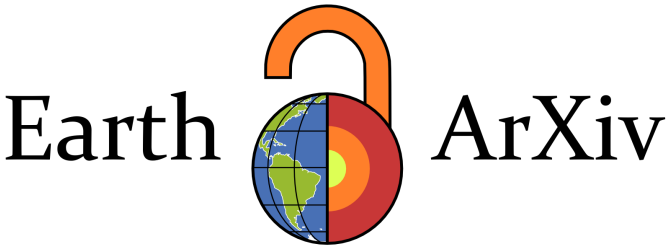

Lowering barriers to probing high-frequency variations in river chemistry through a frugal machine learning-based framework

Amita Prajna Mallik[1,#], Antoine Lucas[1], Eric Gayer[1], Jérôme Gaillardet[1]

[1]Institut de Physique du Globe de Paris, CNRS, Université Paris Cité, 75005 Paris

[#]Corresponding author: **mallik@ipgp.fr**

Peer-review status:

This manuscript is a non-peer reviewed preprint submitted to EarthArXiv.

Lowering barriers to probing high-frequency variations in river chemistry through a frugal machine learning-based framework

Amita Prajna Mallik, Antoine Lucas, Eric Gayer, Jérôme Gaillardet

Institut de Physique du Globe de Paris, CNRS, Université Paris Cité, 75005 Paris

Graphical abstract:

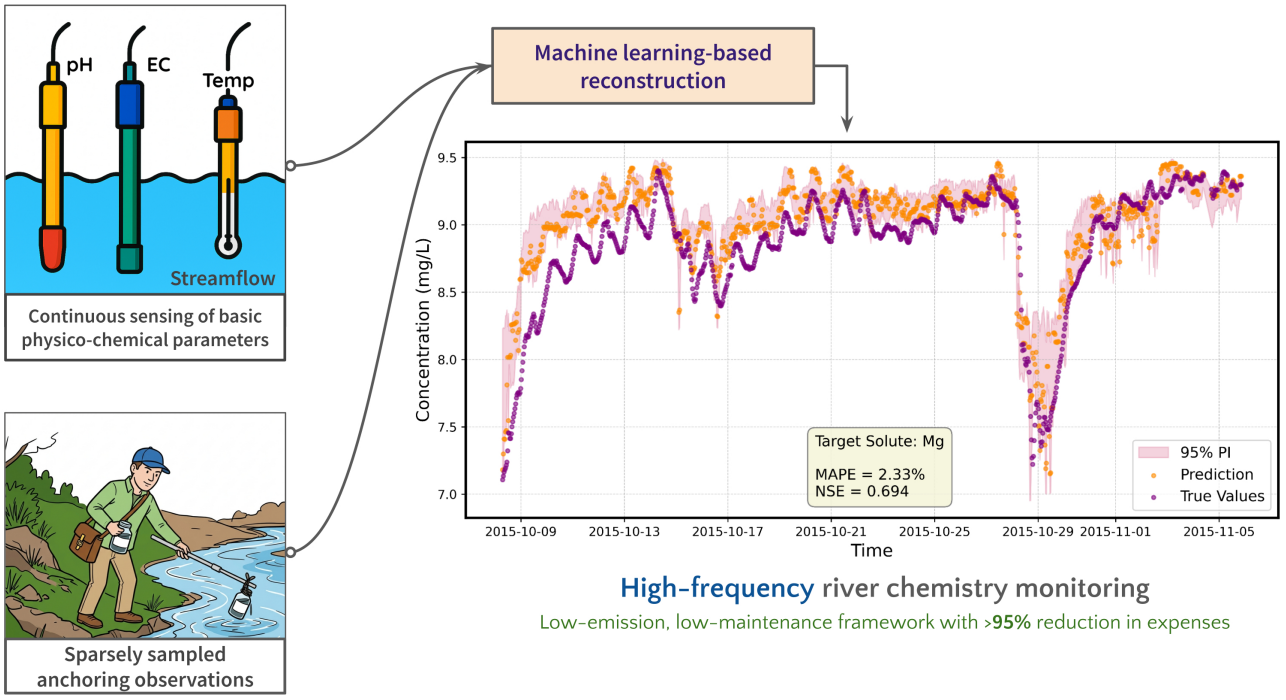

Abstract:

High-frequency river chemistry monitoring is crucial for capturing transient hydro-geochemical variations and ensuring water security, yet its implementation is limited by logistical and budgetary constraints. Here we present a machine learning-based framework that integrates continuous, low-cost physico-chemical proxies with sparse 'anchoring' solute measurements to reconstruct hourly-scale variations in major dissolved metals and nutrients. Validated across three contrasting catchments, we demonstrate that daily to semi-weekly sampling suffice to achieve accurate reconstructions (NSE > 0.75), though sampling demand varies considerably across hydrological regimes. Prediction of nutrients (e.g. NO_3^- and K^+) may require more frequent anchoring observations under stormflow conditions. Reconstruction accuracy is sustained even under multi-week voids in anchoring observations, demonstrating resilience to commonplace logistical disruptions. We complement this framework with a novel gap imputation method based on Singular Spectrum Analysis to address missing data in proxy time series, which outperforms traditional gap-filling approaches. Our results support a scalable, low-maintenance strategy that enables a >95% reduction in operational costs and carbon emissions associated with high-frequency monitoring; and provide a transferable, hydrological regime-specific roadmap for optimizing field sampling that minimizes logistical burden while maintaining reconstruction accuracy.

Introduction

Rivers are the orchestrator of flows in the Earth's critical zone[1], integrating hydrological transport and biogeochemical reactions at the interface between the atmosphere and the continental crust. Incessant anthropogenic inputs of nutrients and contaminants coupled with climatic shifts have disrupted these flows, rendering nearly 80% of the global population vulnerable to water security threats[2].

Monitoring solutes in rivers is crucial to manage the fluvial ecosystems and to support local livelihoods reliant on it. The measurement of major dissolved solutes at a catchment's outlet helps address contaminant flow[3], source apportionment, and the quantification of atmospheric CO_2 consumption by weathering processes[4,5]. While high-frequency monitoring is essential to capture transient hydrochemical changes[6–9], it is often constrained by cost and logistics[10,11]. The conventional method of grab sampling, followed by transportation, storage and laboratory analysis limits the monitoring frequency. Each sample adds to the material, labour and analytical costs, making sustained high-frequency measurements financially challenging. Consequently, low-frequency monitoring lead to erroneous representation of catchment processes - such as undervaluing solute export from watersheds[12] and overlooking drought-induced shifts in nitrate retention[13] or lateral carbon transport[14].

Recent advancements[15–17] through 'lab-in-the-field' setups promise to alleviate these constraints by enabling high-frequency in-situ measurements at accuracies comparable to conventional laboratory measurements. However, adoption remains scant due to their resource and maintenance intensiveness. Solute-specific probes are an emerging cost-effective alternative[18], yet their accuracy and precision can be suboptimal for some analytes[19]. Furthermore, intermittent gaps in observations from inevitable factors such as environmental extremes, sensor fouling or maintenance downtimes exacerbate the data scarcity, impeding downstream modeling and analysis. Common techniques (e.g. linear interpolation, C-Q relationships) used to address these data gaps can occlude the fine-scale temporal variations[20], thus necessitating improved imputation approaches.

The upsurge in adoption of machine learning (ML) has enabled new advancements in hydro-geochemistry, such as short-term forecasting of stream chemistry[21] and insights into drivers of regional-scale water quality[22]. Since monitoring of basic physico-chemical parameters (e.g. pH, Electrical Conductivity (EC), Temperature) is ubiquitous due to affordable sensors,

surrogate modelling combining sensor data with ML holds promise in democratizing high-frequency river chemistry monitoring. These sensors offer near-continuous data, with low operational and labour costs. Prior work has demonstrated success in predicting stream chemistry using surrogate sensor data[23-25]. However, existing studies overlook chemical variability across hydrological regimes and lack rigorous thresholds for when reconstructed data can reliably replace actual solute measurements. Consequently, methodological precedents remain scarce on sustaining predictive skill across hydrological regimes, and during extreme events like storms and droughts.

Collectively, designing a high-frequency river chemistry monitoring framework resilient to observational gaps and unreliant on expensive infrastructure, remains an open research challenge. We aim to address this issue by pursuing three objectives: (a) evaluate whether streamflow and physico-chemical sensors can be used as surrogates for reconstructing solute concentrations across hydrological regimes; and if yes, (b) identify minimum sampling frequencies needed for successful reconstructions; and (c) assess a novel imputation method to address gaps in surrogate time series observations. To achieve these, we use multi-year high-frequency river chemistry measurements from three contrasting catchments, together with accompanying sensor data as surrogates in a ML-based reconstruction framework. The driving hypothesis is that transient variations in stream chemistry can be captured using physico-chemical probes and low-frequency solute measurements.

Materials and Methods

2.1 Study sites and data

The high-frequency river chemistry datasets used in this study were collected from three research watersheds [Fig. 1]: Orgeval (France), Upper Sangamon River Basin (USA) and Plynlimon (UK). These catchments differ in their scale, land use, and geography. While the Orgeval and Sangamon catchments offer solute measurements at sub-hourly resolutions, Plynlimon offers measurements taken every 7 hours.

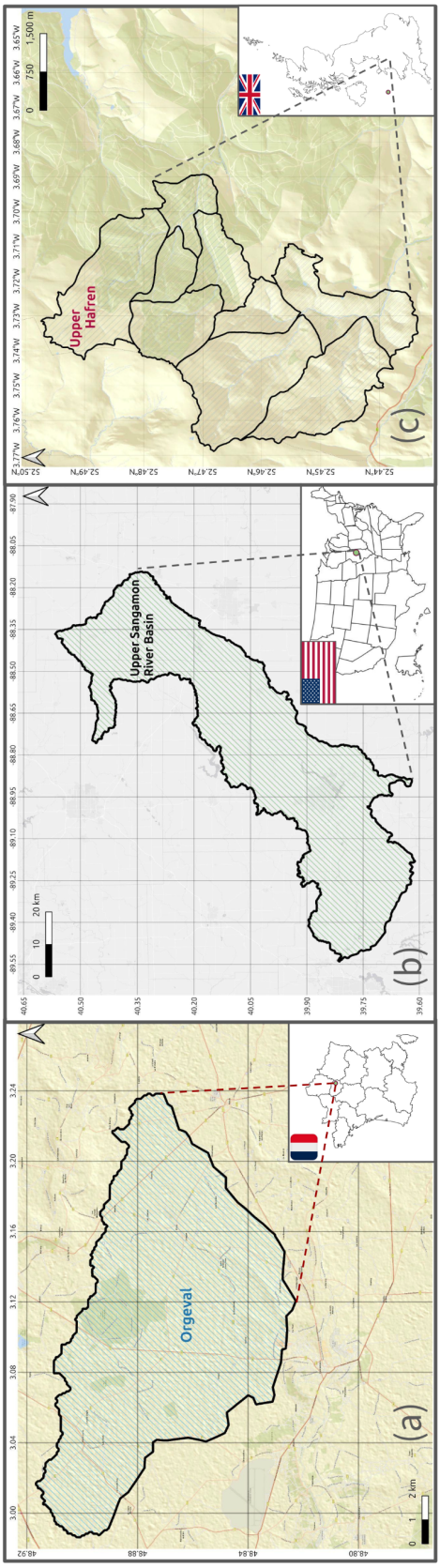

Figure 1: Study sites: (a) Orgeval Critical Zone Observatory, France; (b) Monticello – Upper Sangamon River Basin, USA; (c) Plynlimon research watershed, Wales.

The Avenelles sub-catchment in the Orgeval watershed[26, 27] spans 45 km^2 and is a tile-drained aquifer-fed landscape within the sedimentary carbonate-dominated Paris basin. It consists of horizontally layered limestone, marls, mudstones and silcretes formed at the interface between seawater and coastal plain lakes during the Cenozoic. The local climate is oceanic, with annual average precipitation of 700 mm and average discharge of 0.2 m^3/s (~150 mm/yr) at the outlet. The high-frequency river chemistry data was acquired using a lab-in-the-field setup[17] "RiverLab" [Fig. S1], situated on the Avenelles river at the outlet of the watershed. It continuously samples the stream water and measures the physico-chemical parameters i.e. pH, EC, temperature, turbidity, dissolved organic carbon, and dissolved O_2 through a series of dedicated probes. A portion of this sampled water is routed towards two ThermoFisher Dionex ICS-2100 ion chromatographs, after passing through a filtration system. Here, the dissolved major cations and anions are measured every 40 minutes. The streamflow is recorded using a co-located gauge.

The Upper Sangamon River Basin[28] (hereafter referred to as the Monticello watershed) represents a larger (1500 km^2) agricultural basin on a loess-mantled, glaciated landscape with thick organic-rich soil. It has a humid continental climate, with an average annual precipitation of 1000 mm and average discharge of 10.62 m^3/s (~220 mm/yr) at the outlet. The high-frequency major ion measurements (every 30 minutes) at the outlet of the Sangamon river were obtained using a customized RiverLab system[14], employing Metrohm 940 Professional IC Vario ion chromatographs.

The Upper Hafren watershed[29] from Plynlimon (Wales) was home to one of the earliest efforts in sustained high-frequency river chemistry monitoring. It spans 1.2 km^2, comprising a geology of Lower Palaeozoic slates, mudstones and sandstones influenced by Quaternary glaciation; and is dominated by forests and moorlands. It experiences a humid climate with average annual rainfall of 2600mm and average discharge of 0.1 m^3/s (~2500 mm/yr). The high-frequency sampling was carried out using Xian autosamplers, and samples were measured in the laboratory using ICP-OES for cations and IC for anions.

2.2 Machine learning workflow for stream chemistry reconstruction

We modeled dissolved major solute (Na^+, K^+, Mg^{2+}, Ca^{2+}, SO_4^{2-}, NO_3^-, Cl^-, H_4SiO_4) concentrations using a suite of machine learning algorithms, based on predictors derived from physico-chemical sensor data, streamflow and time [Fig. 2, Text S2].

Figure 2: Summary of the machine learning-based stream chemistry reconstruction approach adopted in this study

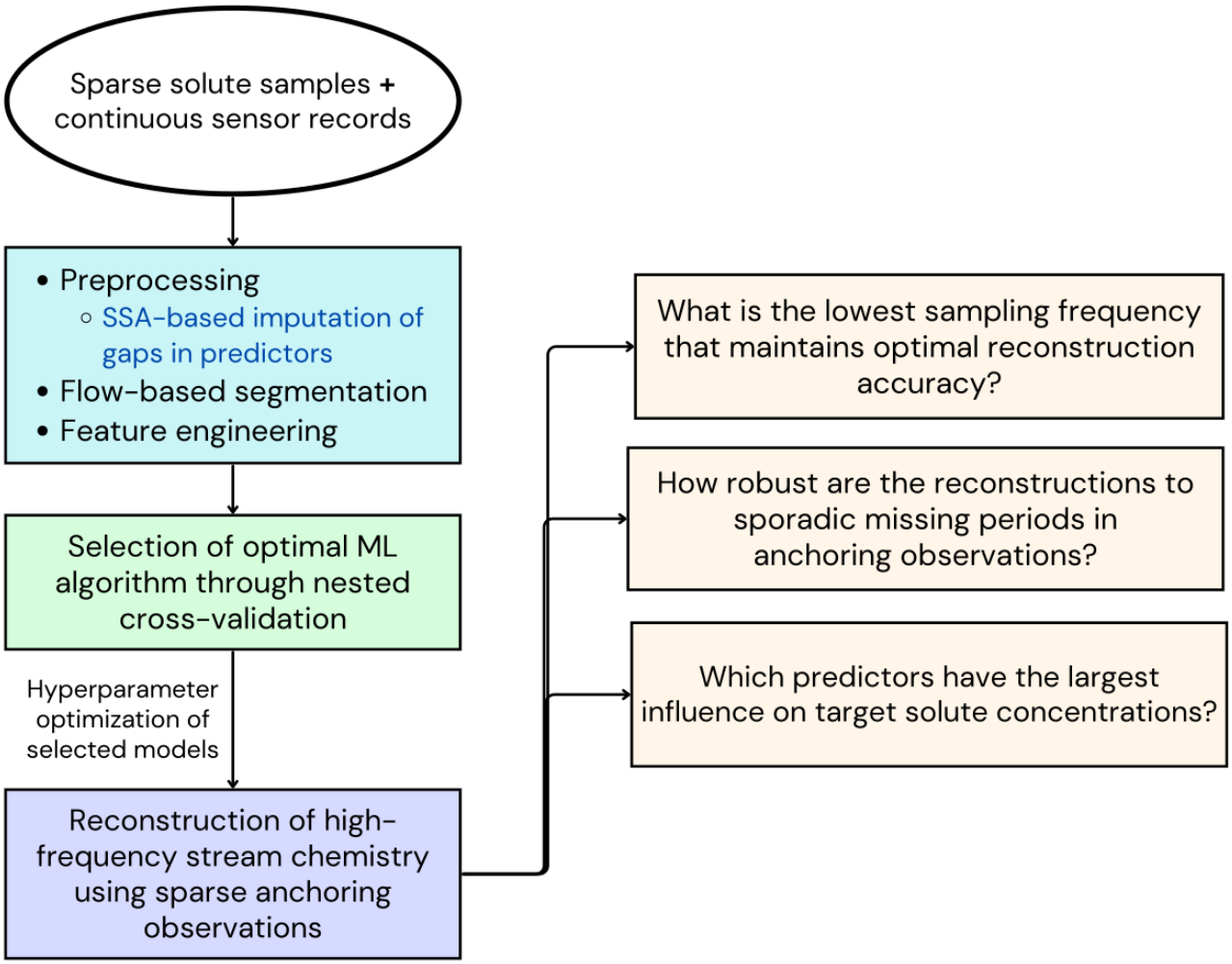

We evaluated several candidate learners [Text S2], including ensemble tree-based algorithms (XGBoost[30], LightGBM[31], Random Forests[32]), regularized linear regression (ElasticNet[33]) and instance-based methods (k-NN[34]), chosen for their interpretability and robustness to uneven sampling. These were trained on sparse, low-frequency subsamples of measured stream chemistry data [Text S4] and corresponding measurements of predictors. To account for hydrochemical variability, separate model instances were trained for each target solute per catchment per hydrological regime (stormflow, transitionary and low flow - delineation detailed in [Text S1]), and additional predictors were formulated to capture diurnality, seasonality, hysteretic behavior and antecedent conditions [Text S2]. The optimal model configuration for each case was selected via nested cross-validation [Text S2], and predictive uncertainty was characterized through quantile regression. The influence of each predictor on the target was quantified using SHapley Additive exPlanations[35] [Text S3]. SHAP attributes an additive importance value to each predictor for every observation, quantifying both the magnitude and direction of a predictor's influence on target solute concentration.

To determine the optimal sampling interval required for accurate high-frequency reconstructions, we trained separate model instances on solute measurements artificially coarsened to lower frequencies and compared their reconstruction performance. Similarly, we evaluated the reconstruction performance under data discontinuity in low-frequency training observations by introducing synthetic gaps of durations ranging from days to months [Text S4].

2.3 Dealing with missing predictors using Singular Spectrum Analysis

Intermittent gaps in sensor data (which are used as predictors) can hinder the reconstruction of high-frequency stream chemistry. We tested a novel method based on Singular Spectrum Analysis[36,37] (SSA) [Text S5] to impute (artificially masked) data gaps in water temperature time series, and compared its efficacy against commonly used imputation techniques. Here, gaps were initially filled using a linear interpolation baseline to create a continuous series. The series was then decomposed into underlying components and reconstructed using dominant components to filter out measurement noise. The missing values were updated using the reconstruction, and the decomposition-reconstruction procedure was conducted iteratively until convergence was reached for the values to be used for gap imputation. For each series, model parameters (window lengths and components used for reconstruction) were calibrated by tuning on artificially created data gaps.

Results and Discussion

3.1 Sampling frequency thresholds and surrogate efficacy for high-frequency stream chemistry reconstruction

[Fig. 3] & [Fig. S6] depict the reconstruction accuracies achieved with "anchoring" low-frequency observations at different intervals. For most solutes across the three catchments, anchoring measurements at daily to semi-weekly sampling intervals suffice to obtain accurate hourly-scale reconstructions (evidenced by Nash-Sutcliffe Efficiency > 0.75). Comparable accuracies at the Monticello catchment obtained using weekly (or sparser) sampling suggest that even lower frequencies could be viable, but testing this for other catchments was beyond this study's scope due to insufficient training data at coarser intervals. Generally, sub-daily (or higher) sampling yielded negligible accuracy improvements to justify the increased logistical burden.

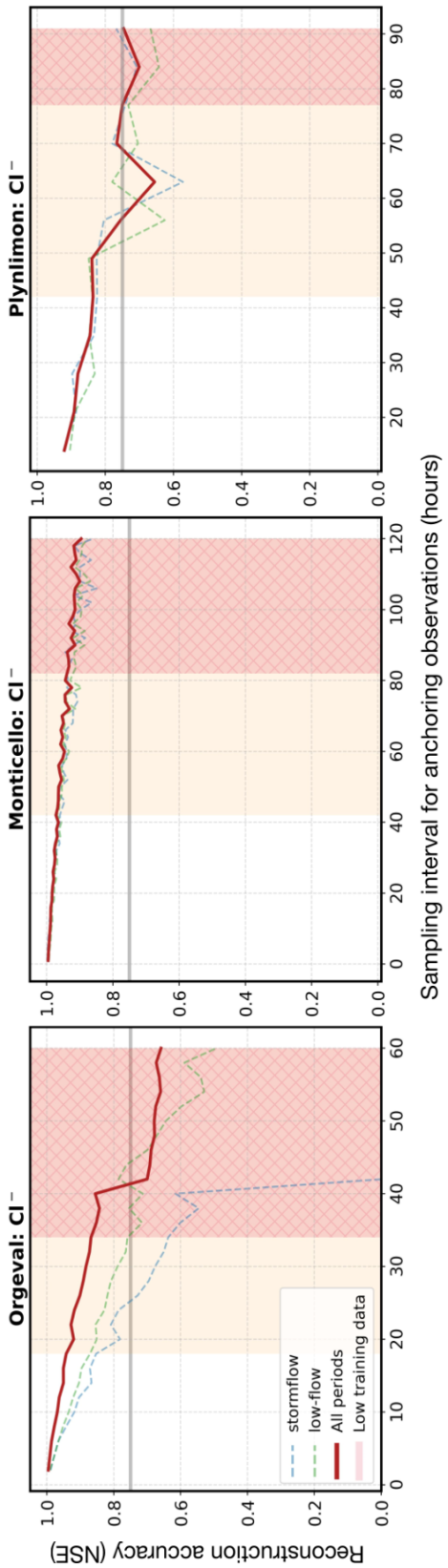

Figure 3: Illustration depicting reconstruction accuracy of high-frequency (hourly at Orgeval/Monticello & 7-h at Plynlimon) Cl^- concentrations against various intervals at which anchoring observations were used to train the model. Blue and green dashed lines denote reconstruction performance for stormflow and low-flow periods respectively, and thick red line represents all periods (including transitionary flow) pooled together. Accuracy is quantified using Nash-Sutcliffe Efficiency, with values greater than 0.75 (depicted via horizontal grey line) considered a threshold for optimal predictions. Yellow (<100 observations) and checkered red background (<50 observations) shading indicate severity of insufficiency in training data, leading to degraded model predictions. This plot considers a representative solute [Cl^-], and the results for whole suite of solutes is provided in [Text S4, Fig. S6]

For a given anchoring frequency, the observed differences in reconstruction accuracy across hydrological regimes reinforce the need for regime-specific monitoring and modelling approaches. Relative to baseflow periods, a denser sampling effort is required to maintain comparable accuracies during stormflow periods. This sampling demand is exacerbated in small catchments (Plynlimon and Orgeval) with short hydrological response times, in contrast to large catchments (Monticello) where the hydrological response is attenuated[38]. Additionally, we reason that for certain solutes (e.g. NO_3^-, K^+) which are often present in superficial soil layers and are mobilized through shallow, rapid flowpaths, low-frequency monitoring fails to adequately characterize [Fig. S6] the antecedent conditions that govern their delivery during storm events.

[Fig. S2, S3-S5] elucidate the impact of each predictor on target solute concentration by employing SHAP values. Acknowledging the drawbacks of this approach in making causal inferences[39], here we summarize first-order interpretations of dominant predictor-target relationships. EC, which is a proxy for total dissolved solutes, consistently acts as an influential predictor for most major solutes. EC embeds information regarding individual solutes[25], that can be effectively utilized to reconstruct target solute concentrations even in catchments with markedly different river chemistries. Streamflow is another primary control on dissolved solute concentrations, consistent with the idea of water residence time being an important determinant of solute fluxes from landscapes[40]. Additionally, the prediction of nutrients such as NO_3^- & K^+ is aided by a proxy corresponding to seasonality signifying their active role in biological cycling. A detailed treatment of the role of other predictors on each target solute, across regime-catchment combinations is provided in [Text S3, Fig. S3-S5].

3.2 Reconstruction performance under missing periods in anchoring observations

The proposed reconstruction approach hinges on two requisites: continuous sensor data and low-frequency anchoring observations. For robust practical deployment, it is necessary for the approach to be resilient to prolonged missing periods in anchoring observations which may arise due to adverse weather or labour shortfall. [Figure 4] depicts the reconstruction accuracy (mean absolute percentage error, or MAPE) during periods with extended gaps in anchoring observations, ranging from 1 day to 30 days. For most solutes, the errors stay within 2-5% in the Orgeval catchment, and within 2-7% in the Plynlimon catchment – even during month-long data voids. Monticello catchment was not analyzed due to insufficient temporally contiguous segments needed to simulate large data gaps.

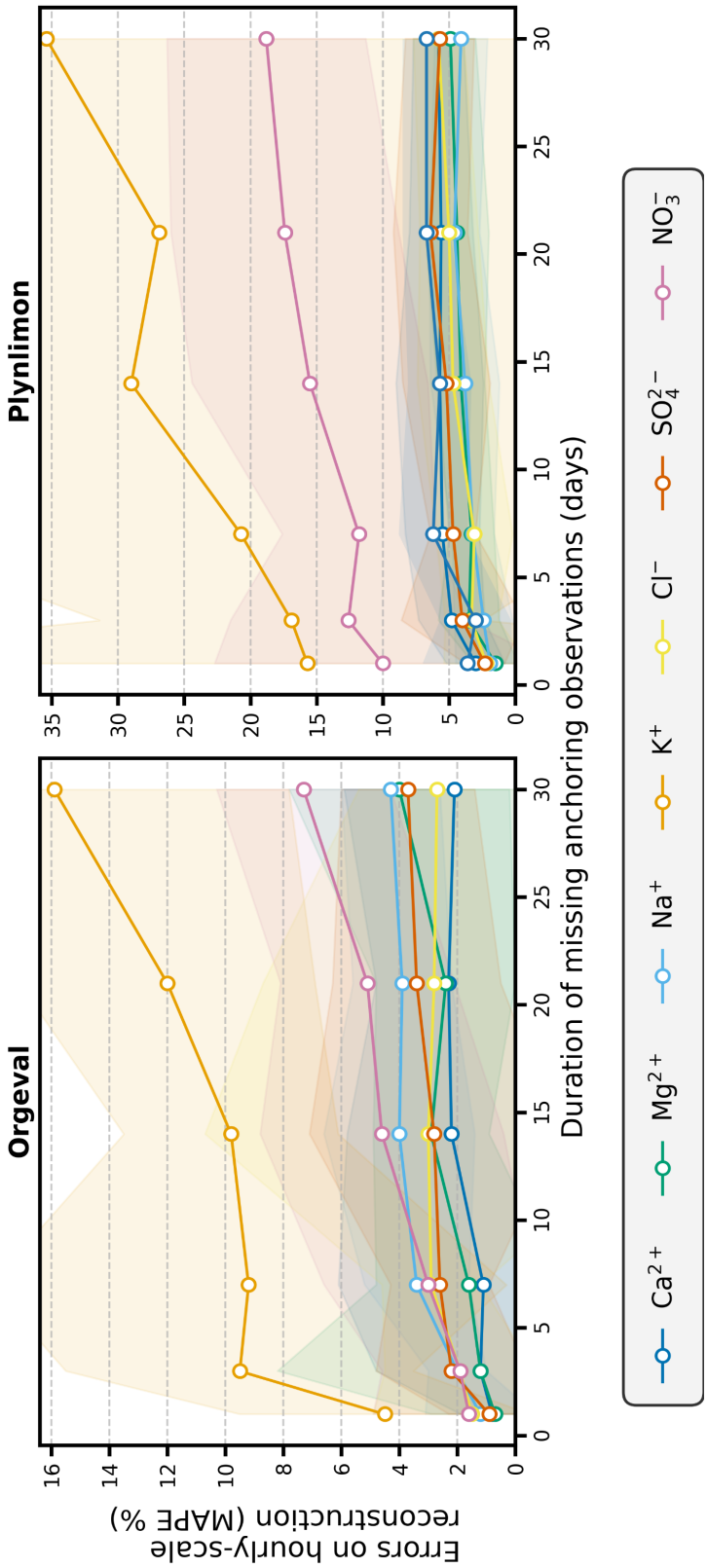

Figure 4: Evaluation of reconstruction accuracy (quantified using mean absolute percentage error, MAPE) under varying durations of missing periods in anchoring observations. In other words, it depicts the duration till which predictions can be made reliably even in the absence of low-frequency anchoring observations. Uncertainty bounds are reported using standard deviation of prediction accuracy over 20 randomly chosen, non-overlapping segments. Results shown for Orgeval and Plynlimon; Monticello not analyzed due to lack of sufficient contiguous segments necessary to simulate extended data gaps.

The instances of degraded reconstruction accuracy for NO_3^- and K^+ likely stem from their role in biological cycling and enrichment in upper soil horizons of the catchment – due to processes such as fertilizer application, atmospheric deposition or decaying organic matter[41]. Without preceding data to constrain these transient nutrient pools and the antecedent conditions, the model's 'memory' to simulate solute delivery processes is constrained. This is also reflected in the high variability in C-Q relationships of these solutes, exhibiting complex hysteretic behavior that is difficult to capture without frequent observations.

Despite this, the framework's broader performance indicates that the learned relationships are sufficiently robust to bridge multi-week observational voids for most major ions.

3.3 Maintaining temporal integrity in predictor time series during sensor downtimes

[Figure S7] depicts the superior performance of SSA-based approach in retaining the original predictor signal's variability and temporal structure during gap imputation. Conventional imputation methods (linear/spline interpolation, ARIMA) either act as low-pass filters muting fine-scale variations, or assume stationarity that is seldom satisfied by environmental time series. Since the reconstruction of solutes is contingent on continuous availability of predictor time series, errors arising from suboptimal gap-filling in predictor time series can propagate into solute predictions. We thus suggest that the adoption of this method will improve the fidelity of the reconstructions in case of data voids in predictors.

Implications & Conclusion

River chemistry is a key component of long-term environmental observatories[42,43] that contributes to a holistic understanding of ecosystem functioning. However, the continuous power demand of chromatographic measurements, consumable usage and site interventions contribute to the operational costs and carbon footprint of the monitoring infrastructures, often operating under existing logistical and budgetary constraints. Here we show that passive, low-power sensors and strategically timed anchoring observations democratize high-frequency monitoring without relying on expensive infrastructure. This hybrid strategy provides a significant reduction in net atmospheric CO_2 emissions and a ~95% reduction in operational costs [Text S6], especially when cumulated over long-term monitoring campaigns across multiple sites. Therefore, the study lays a foundation for sustained high-frequency river chemistry monitoring that is aligned with broader climate mitigation goals without compromising on spatiotemporal resolution.

References

1. US National Research Council. (2001). Basic Research Opportunities in Earth Science. National Academies Press. https://doi.org/10.17226/9981
2. Vörösmarty, C. J., McIntyre, P. B., Gessner, M. O., Dudgeon, D., Prusevich, A., Green, P., Glidden, S., Bunn, S. E., Sullivan, C. A., Liermann, C. R., & Davies, P. M. (2010). Global threats to human water security and river biodiversity. Nature, 467(7315), 555–561. https://doi.org/10.1038/nature09440
3. Smith, R. A., Alexander, R. B., & Wolman, M. G. (1987). Water-Quality Trends in the Nation's Rivers. Science, 235(4796), 1607–1615. https://doi.org/10.1126/science.235.4796.1607
4. Gaillardet, J., Dupré, B., Louvat, P., & Allègre, C. J. (1999). Global silicate weathering and CO2 consumption rates deduced from the chemistry of large rivers. Chemical Geology, 159(1–4), 3–30. https://doi.org/10.1016/S0009-2541(99)00031-5
5. Chen, C., Gayer, E., Gaillardet, J., Derry, L. A., Louvat, P., Bouchez, J., Jin, Z., & Yokochi, R. (2025). Enhanced weathering by multiscale destabilization of volcanic islands. Earth and Planetary Science Letters, 671, 119649. https://doi.org/10.1016/j.epsl.2025.119649
6. Heathwaite, A. L., & Bieroza, M. (2021). Fingerprinting hydrological and biogeochemical drivers of freshwater quality. Hydrological Processes, 35(1), e13973. https://doi.org/10.1002/hyp.13973
7. Kirchner, J. W., Feng, X., Neal, C., & Robson, A. J. (2004). The fine structure of water-quality dynamics: The (high-frequency) wave of the future. Hydrological Processes, 18(7), 1353–1359. https://doi.org/10.1002/hyp.5537
8. Skeffington, R. A., Halliday, S. J., Wade, A. J., Bowes, M. J., & Loewenthal, M. (2015). Using high-frequency water quality data to assess sampling strategies for the EU Water Framework Directive. Hydrology and Earth System Sciences, 19(5), 2491–2504. https://doi.org/10.5194/hess-19-2491-2015
9. Bieroza, M., Acharya, S., Benisch, J., Ter Borg, R. N., Hallberg, L., Negri, C., Pruitt, A., Pucher, M., Saavedra, F., Staniszewska, K., Van'T Veen, S. G. M., Vincent, A., Winter, C., Basu, N. B., Jarvie, H. P., & Kirchner, J. W. (2023). Advances in Catchment Science, Hydrochemistry, and Aquatic Ecology Enabled by High-Frequency Water Quality Measurements. Environmental Science & Technology, 57(12), 4701–4719. https://doi.org/10.1021/acs.est.2c07798
10. Rozemeijer, J., Jordan, P., Hooijboer, A., Kronvang, B., Glendell, M., Hensley, R., Rinke, K., Stutter, M., Bieroza, M., Turner, R., Mellander, P. E., Thorburn, P., Cassidy, R., Appels, J., Ouwerkerk, K., & Rode, M. (2025). Best practice in high-frequency water quality monitoring for improved management and assessment; a novel decision workflow. Environmental Monitoring and Assessment, 197(4), 353. https://doi.org/10.1007/s10661-025-13795-z
11. Brekenfeld, N., Cotel, S., Faucheux, M., Fourtet, C., Hamon, Y., Petitjean, P., Blanchouin, A., Bouillis, C., Pierret, M.-C., Henine, H., Pierson-Wickmann, A.-C., Guillon, S., Floury, P., & Fovet, O. (2025). Technical note: High-frequency, multi-elemental stream water monitoring – experiences, feedbacks and suggestions from 7 years of running three French field laboratories (Riverlabs). Hydrology and Earth System Sciences, 29(12), 2615–2631. https://doi.org/10.5194/hess-29-2615-2025
12. Moatar, F., Meybeck, M., Raymond, S., Birgand, F., & Curie, F. (2013). River flux uncertainties predicted by hydrological variability and riverine material behaviour. Hydrological Processes, 27(25), 3535–3546. https://doi.org/10.1002/hyp.9464

13. Winter, C., Nguyen, T. V., Musolff, A., Lutz, S. R., Rode, M., Kumar, R., & Fleckenstein, J. H. (2023). Droughts can reduce the nitrogen retention capacity of catchments. Hydrology and Earth System Sciences, 27(1), 303–318. https://doi.org/10.5194/hess-27-303-2023

14. Wang, J., Bouchez, J., Winnick, M. J., Goodwell, A. E., Dere, A., Kumar, P., & Druhan, J. L. (2025). Drought constrictions on lateral carbon transport. Nature Geoscience, 18(11), 1138–1143. https://doi.org/10.1038/s41561-025-01807-z

15. Stravs, M. A., Stamm, C., Ort, C., & Singer, H. (2021). Transportable Automated HRMS Platform "MS2 field" Enables Insights into Water-Quality Dynamics in Real Time. Environmental Science & Technology Letters, 8(5), 373–380. https://doi.org/10.1021/acs.estlett.1c00066

16. Rode, M., Wade, A. J., Cohen, M. J., Hensley, R. T., Bowes, M. J., Kirchner, J. W., Arhonditsis, G. B., Jordan, P., Kronvang, B., Halliday, S. J., Skeffington, R. A., Rozemeijer, J. C., Aubert, A. H., Rinke, K., & Jomaa, S. (2016). Sensors in the Stream: The High-Frequency Wave of the Present. Environmental Science & Technology, 50(19), 10297–10307. https://doi.org/10.1021/acs.est.6b02155

17. Floury, P., Gaillardet, J., Gayer, E., Bouchez, J., Tallec, G., Ansart, P., Koch, F., Gorge, C., Blanchouin, A., & Roubaty, J.-L. (2017). The potamochemical symphony: New progress in the high-frequency acquisition of stream chemical data. Hydrology and Earth System Sciences, 21(12), 6153–6165. https://doi.org/10.5194/hess-21-6153-2017

18. Meyer, A. M., Oliveri, E., Kautenburger, R., Hein, C., Kickelbick, G., & Beck, H. P. (2025). In situ real-time monitoring of ammonium, potassium, chloride and nitrate in small and medium-sized rivers using ion-selective-electrodes – a case study of feasibility. Environmental Science: Advances, 4(8), 1238–1249. https://doi.org/10.1039/D5VA00021A

19. Salgado, R., & Simoes, M. (2013). Chromatographic, Polarographic and Ion-Selective Electrodes Methods for Chemical Analysis of Groundwater Samples in Hydrogeological Studies. In M. Khalid (Ed.), Electrochemistry. InTech. https://doi.org/10.5772/50223

20. Wang, J., Bouchez, J., Dolant, A., Floury, P., Stumpf, A. J., Bauer, E., Keefer, L., Gaillardet, J., Kumar, P., & Druhan, J. L. (2024). Sampling frequency, load estimation and the disproportionate effect of storms on solute mass flux in rivers. Science of The Total Environment, 906, 167379. https://doi.org/10.1016/j.scitotenv.2023.167379

21. Agrawal, T., Goodwell, A., & Kumar, P. (2025). Improving Stream Solute Predictions With a Modified LSTM Model Incorporating Solute Interdependences and Hysteresis Patterns. Journal of Geophysical Research: Machine Learning and Computation, 2(1), e2024JH000383. https://doi.org/10.1029/2024JH000383

22. Goldrich-Middaugh, G. M., Johnson, K., Ma, L., Engle, M. A., Fleming, S. W., Ricketts, J. W., & Sullivan, P. L. (2025). Critical zone controls on stream chemistry: Lessons from multiple machine learning methods and irregular data across large watersheds. Journal of Hydrology, 660, 133319. https://doi.org/10.1016/j.jhydrol.2025.133319

23. Green, M. B., Pardo, L. H., Bailey, S. W., Campbell, J. L., McDowell, W. H., Bernhardt, E. S., & Rosi, E. J. (2021). Predicting high-frequency variation in stream solute concentrations with water quality sensors and machine learning. Hydrological Processes, 35(1), e14000. https://doi.org/10.1002/hyp.14000

24. Harrison, J. W., Lucius, M. A., Farrell, J. L., Eichler, L. W., & Relyea, R. A. (2021). Prediction of stream nitrogen and phosphorus concentrations from high-frequency sensors using Random Forests Regression. Science of The Total Environment, 763, 143005. https://doi.org/10.1016/j.scitotenv.2020.143005

25. Benettin, P., & Van Breukelen, B. M. (2017). Decomposing the Bulk Electrical Conductivity of Streamflow To Recover Individual Solute Concentrations at High Frequency. Environmental Science & Technology Letters, 4(12), 518–522. https://doi.org/10.1021/acs.estlett.7b00472

26. Floury, P., Gaillardet, J., Tallec, G., Ansart, P., Bouchez, J., Louvat, P., & Gorge, C. (2019). Chemical weathering and CO2 consumption rate in a multilayered-aquifer dominated watershed under intensive farming: The Orgeval Critical Zone Observatory, France. Hydrological Processes, 33(2), 195–213. https://doi.org/10.1002/hyp.13340

27. Floury, P., Bouchez, J., Druhan, J. L., Gaillardet, J., Blanchouin, A., Gayer, É., & Ansart, P. (2024). Linking Dynamic Water Storage and Subsurface Geochemical Structure Using High-Frequency Concentration-Discharge Records. Water Resources Research, 60(1), e2022WR033999. https://doi.org/10.1029/2022WR033999

28. Wilson, C. G., Abban, B., Keefer, L. L., Wacha, K., Dermisis, D., Giannopoulos, C., Zhou, S., Goodwell, A. E., Woo, D. K., Yan, Q., Ghadiri, M., Stumpf, A., Pitcel, M., Lin, Y.-F., Marini, L., Storsved, B., Goff, K., Vogelgsang, J., Dere, A., … Papanicolaou, A. N. (2018). The Intensively Managed Landscape Critical Zone Observatory: A Scientific Testbed for Understanding Critical Zone Processes in Agroecosystems. Vadose Zone Journal, 17(1), 1–21. https://doi.org/10.2136/vzj2018.04.0088

29. Neal, C., Reynolds, B., Kirchner, J. W., Rowland, P., Norris, D., Sleep, D., Lawlor, A., Woods, C., Thacker, S., Guyatt, H., Vincent, C., Lehto, K., Grant, S., Williams, J., Neal, M., Wickham, H., Harman, S., & Armstrong, L. (2013). High-frequency precipitation and stream water quality time series from Plynlimon, Wales: An openly accessible data resource spanning the periodic table. Hydrological Processes, 27(17), 2531–2539. https://doi.org/10.1002/hyp.9814

30. Chen, T., & Guestrin, C. (2016). XGBoost: A Scalable Tree Boosting System. Proceedings of the 22nd ACM SIGKDD International Conference on Knowledge Discovery and Data Mining, 785–794. https://doi.org/10.1145/2939672.2939785

31. Ke, G., Meng, Q., Finley, T., Wang, T., Chen, W., Ma, W., Ye, Q., & Liu, T.-Y. (2017). LightGBM: a highly efficient gradient boosting decision tree. Proceedings of the 31st International Conference on Neural Information Processing Systems, NIPS'17, 3149–3157.

32. Breiman, L. (2001). Random Forests. Machine Learning, 45(1), 5–32. https://doi.org/10.1023/A:1010933404324

33. Zou, H., & Hastie, T. (2005). Regularization and Variable Selection Via the Elastic Net. Journal of the Royal Statistical Society Series B: Statistical Methodology, 67(2), 301–320. https://doi.org/10.1111/j.1467-9868.2005.00503.x

34. Fix, E., & Hodges, J. L. (1951). Discriminatory Analysis. Nonparametric Discrimination: Consistency Properties. International Statistical Review / Revue Internationale de Statistique, 57(3), 238. https://doi.org/10.2307/1403797

35. Lundberg, S., & Lee, S.-I. (2017). A Unified Approach to Interpreting Model Predictions (Version 2). arXiv. https://doi.org/10.48550/ARXIV.1705.07874

36. Vautard, R., Yiou, P., & Ghil, M. (1992). Singular-spectrum analysis: A toolkit for short, noisy chaotic signals. Physica D: Nonlinear Phenomena, 58(1–4), 95–126. https://doi.org/10.1016/0167-2789(92)90103-T

37. Delforge, D., Alonso, A., De Viron, O., Vanclooster, M., & Speybroeck, N. (2025). SSALib: A Python Library for Time Series Decomposition using Singular Spectrum Analysis. Journal of Open Source Software, 10(115), 8600. https://doi.org/10.21105/joss.08600

38. Macdonald, E., Merz, B., Guse, B., Wietzke, L., Ullrich, S., Kemter, M., Ahrens, B., & Vorogushyn, S. (2022). Event and Catchment Controls of Heavy Tail Behavior of Floods. Water Resources Research, 58(6), e2021WR031260. https://doi.org/10.1029/2021WR031260

39. Kumar, I. E., Venkatasubramanian, S., Scheidegger, C., & Friedler, S. (2020). Problems with Shapley-value-based explanations as feature importance measures. In H. D. III & A. Singh (Eds.), Proceedings of the 37th International Conference on Machine Learning (Vol. 119, pp. 5491–5500). PMLR. https://proceedings.mlr.press/v119/kumar20e.html

40. Maher, K. (2011). The role of fluid residence time and topographic scales in determining chemical fluxes from landscapes. Earth and Planetary Science Letters, 312(1–2), 48–58. https://doi.org/10.1016/j.epsl.2011.09.040

41. Garnier, J., Billen, G., Vilain, G., Benoit, M., Passy, P., Tallec, G., Tournebize, J., Anglade, J., Billy, C., Mercier, B., Ansart, P., Azougui, A., Sebilo, M., & Kao, C. (2014). Curative vs. preventive management of nitrogen transfers in rural areas: Lessons from the case of the Orgeval watershed (Seine River basin, France). Journal of Environmental Management, 144, 125–134. https://doi.org/10.1016/j.jenvman.2014.04.030

42. Gaillardet, J., Braud, I., Hankard, F., Anquetin, S., Bour, O., Dorfliger, N., De Dreuzy, J. R., Galle, S., Galy, C., Gogo, S., Gourcy, L., Habets, F., Laggoun, F., Longuevergne, L., Le Borgne, T., Naaim-Bouvet, F., Nord, G., Simonneaux, V., Six, D., … Zitouna, R. (2018). OZCAR: The French Network of Critical Zone Observatories. Vadose Zone Journal, 17(1), 1–24. https://doi.org/10.2136/vzj2018.04.0067

43. Zacharias, S., Loescher, H. W., Bogena, H., Kiese, R., Schrön, M., Attinger, S., Blume, T., Borchardt, D., Borg, E., Bumberger, J., Chwala, C., Dietrich, P., Fersch, B., Frenzel, M., Gaillardet, J., Groh, J., Hajnsek, I., Itzerott, S., Kunkel, R., … Vereecken, H. (2024). Fifteen Years of Integrated Terrestrial Environmental Observatories (TERENO) in Germany: Functions, Services, and Lessons Learned. Earth's Future, 12(6), e2024EF004510. https://doi.org/10.1029/2024EF004510

Supporting information

Lowering barriers to probing high-frequency variations in river chemistry through a frugal machine learning-based framework

Amita Prajna Mallik, Antoine Lucas, Eric Gayer, Jérôme Gaillardet

Institut de Physique du Globe de Paris, CNRS, Université Paris Cité, 75005 Paris

---

Contents

S1. Data acquisition and preprocessing

S1.1 Orgeval

The dataset from Orgeval catchment used in this study is available at [Ansart et. al. 2020] and via the website: https://bdoh.irstea.fr/ORACLE/. The data had undergone QA/QC checks following the procedure detailed in [Floury et. al. 2017], and the period of interest was confined to 2015–2017 to ensure minimal disruptions in contiguous data availability. We limited our analysis to the following columns: major solutes (Ca, Mg, Na, K, Cl, SO_4, NO_3), physico-chemical sensor measurements (pH, Temperature, Electrical Conductivity, Dissolved O_2), Discharge and time. The temperature values from the period of 12-09-2015 to 07-10-2015 appeared to exhibit consistent anomalously high values, which was corrected by computing and subtracting an offset. The final dataset consisted of 20,320 rows that had atleast one valid major solute observation, and the median interval between consecutive solute measurements was 41 minutes.

S1.2 Monticello

The data from the Monticello watershed used in this study is publicly available through the supplementary material contained in [Wang et. al., 2025], having undergone prior data cleaning and quality control. We confined our analysis to the same set of major solutes, discharge and physico-chemical sensor measurements (except pH, which was unavailable for the catchment) over a period between 2021–2023. The median interval between consecutive solute measurements was 29 minutes, and the dataset consisted of 22,526 rows with at least one valid solute measurement.

S1.3 Plynlimon

The data from the Upper Hafren subcatchment of the Plynlimon research watershed used in this study is publicly available at [Neal et. al. 2013]. The data was collected over a period of 2007–2009, and we confined our analysis to the previously listed set of columns (except dissolved O_2, which was unavailable at the catchment). Consecutive observations were taken at a 7-hour interval, and the dataset consisted of 2085 valid measurements of interest.

S1.4 Delineation of hydrological periods from discharge data

To account for the fact that solute delivery to the stream varies significantly with flow conditions, we partitioned the hydrograph into three hydrological regimes: stormflow, transitionary flow and low-flow [Fig. S9]. Storm events were delineated using a custom algorithm (available in the supplementary codes), that starts by applying a rolling window mean to smooth high-frequency noise from the hydrograph. Local maxima were then identified using a prominence-based peak detection function, with minimum prominence and storm duration threshold as adjustable parameters tuned for each catchment. Clusters of peaks within the storm duration threshold were grouped under a single storm event, with the highest discharge value within each cluster defined as the event peak. The start and end points of each storm event were defined by searching for the local minima - backward from the first peak, and forward from the final peak. After identification of the storm events (which were pooled together as stormflow), remaining non-storm data were separated into baseflow and transitionary flow based on a percentile threshold deduced from visual inspection. For the Plynlimon catchment, all non-storm periods were pooled into low-flow period due to limited data availability for further segmentation.

S2. Model selection, optimization and feature engineering for stream chemistry reconstruction

The machine learning workflow for stream chemistry reconstruction started by defining the set of predictor variables. The base set of predictors consisted of the available physico-chemical sensor data (EC, pH, Temperature and dissolved O_2), streamflow and time-derived predictors. Temporal features consisting of a value between 0 and 1 were used to represent diurnal and seasonal cycles, referred to as DayIndex and YearIndex respectively. For better prediction of stormflow periods, hydrologically-informed predictors were added to this base set. These consisted of within-storm normalized discharge, instantaneous slope of hydrograph and a binary limb type indicator (ascending/descending), contributing to better capturing of the hysteretic behaviour observed in event-scale concentration-discharge relationships. Additionally, 24-hour antecedent conductivity was used as a predictor [Knapp et. al. 2020] to account for the catchment's event-scale chemical 'memory'.

Each target solute-hydrological regime combination across catchments was modeled separately due to differences in origin, transport and reactivity of the solutes. The selection of the optimal machine learning algorithm for each solute-regime combination from a set of candidate learners was performed using a nested cross-validation procedure. In this, the outer loop iteratively splits the data into training and testing sets, to estimate the generalization error on unseen data. The inner loop works within the training set of a given outer loop, evaluating multiple candidate models. Here, the root mean square error (RMSE) is used as the objective function, and the model with the lowest mean RMSE across inner cross-validation loops is chosen as the best model for the outer fold. Next, the selected model is retrained on the entire outer training set and evaluated on the outer test set. After completing all the outer cross-validation loops, the overall best model for the solute-period combination is determined by selecting the most frequently chosen model across the outer folds. In case of a tie, the model with the lowest average outer RMSE is selected. The best models chosen for each target-period combination in Orgeval catchment are shown below (Table S1):

	Stormflow	**Transitionary**	**Baseflow**
Ca^{2+}	Random Forest	Random Forest	XGBoost
Mg^{2+}	LightGBM	XGBoost	XGBoost

Na^+	LightGBM	XGBoost	Random Forest
K^+	Random Forest	Random Forest	Random Forest
Cl^-	LightGBM	XGBoost	XGBoost
SO_4^{2-}	LightGBM	XGBoost	Random Forest
NO_3^-	LightGBM	Random Forest	XGBoost

After chosing the best algorithm for each solute-period-catchment combination, we used an automated hyperparameter optimization framework, Optuna [Akiba et. al. 2019] to adjust the model hyperparameters (hyperparameters are the external variables used to configure the model training process). It is useful to note here that hyperparameter optimization yielded marginal improvements in prediction accuracy, and may be omitted in use cases where simplicity and/or computational efficiency is paramount.

If an user desires simplicity in algorithm selection (without the computationally expensive nested cross-validation procedure), we suggest that XGBoost may be selected as the default algorithm. This algorithm consistently demonstrated high accuracy across each catchment-period-target combination, and while it might not have been the most accurate for each case, its accuracy was comparable to (and closely behind) the top-performing algorithm for each combination. In tune with this, we chose to work with XGBoost for all period-target combinations for the Monticello and Plynlimon catchments.

While deep learning algorithms such as LSTMs, Transformers can be a powerful alternative for time series prediction, they were not considered here as candidate learners due to their limited interpretability; and because observational gaps/uneven sampling intervals typical to river chemistry datasets hinder their applicability.

S3. **Quantifying the relative influence of predictors**

To estimate the marginal contribution of different predictors on a target solute for a given period, a game-theoretic approach called Shapley Additive Explanations (SHAP) framework was used. SHAP assigns an 'additive importance' value to each feature for every individual data point, quantifying both the magnitude and the direction (positive or negative) of its influence on the predicted concentration. This allows for a granular assessment of how predictors (such as conductivity or temperature) shift target solute concentrations across different hydrological regimes.

SHAP summary plots are used to visualize the distribution of these influences. Each point on the plot represents an individual observation, where the position on the x-axis indicates whether the predictor's value increased or decreased the predicted concentration, and the color represents the predictor's magnitude. In figures S3-S5, we present the catchment-wise SHAP summary plots for each target solute, across stormflow and baseflow periods.

A first-order overview of the SHAP analyses presented in figures S3-S5 is shown in figure S2. To create this summary, the SHAP plot for each target-period-catchment combination was studied, and a scoring method was undertaken where the top 3 predictors were assigned a score of 1, 0.66 and 0.33 respectively. Then for each period-catchment combination, the scores obtained by each predictor were averaged across multiple target solutes. These averaged values were normalized to a value between 0 and 1 (for each catchment-period combination), to get an approximate measure of the influence of each predictor on solute predictions. A positive/negative value (indicated by the cell color in Fig. S2) was assigned based on an average direction of influence i.e. whether an increase in predictor values, on an average, led to an increase or decrease (respectively) in solute concentrations. Note that this exercise is purely a first-order approximation that overlooks the heterogeneities in predictor-target relationship across different target solutes.

S4. **Sensitivity analysis to sampling frequency**

The sensitivity of the reconstruction accuracy to varying frequencies of anchoring observations was simulated by artificially coarsening the high-frequency river chemistry data. The models were trained separately on temporal subsamples mimicking lower sampling intervals (ranging upto 120 hours, depending on the catchment). Then, these models trained on low-frequency observations were used to predict the high-frequency river chemistry consistent with the original resolution of observations. Reconstruction accuracy was quantified using Nash-Sutcliffe Efficiency (NSE). [Fig. S6] depicts the reconstruction accuracy at varying sampling frequencies, for each catchment-period-ion combination.

The scope of the sensitivity tests was constrained by the original lengths of the high-frequency time series. Since these tests were performed by subsampling the original observations, testing very sparse anchoring frequencies (e.g. measurements taken at weekly or monthly intervals) was not feasible. This is because the training set becomes too small for the machine learning algorithm to achieve reliable generalization performance.

S4.1 Out-of-distribution reconstruction performance

The approach taken in this work is that of conditional reconstruction, relying on the assumption of piecewise stationarity to perform reconstructions as long as there are training (anchoring) data to constraint the antecedent and future conditions on both sides of the interval to be reconstructed. This is different from assuming stationarity for a given solute-catchment-hydrological regime combination, in which case it should be possible to make hindcasts/forecasts without any anchoring observations. Hence, it is worth noting that predictions outside training temporal range may be suboptimal due to the non-stationarity inherent to river chemistry time series. However, we do not discuss that aspect in this work since our focus is on “interpolating” between sparse training samples.

While we work under the assumptions of piecewise stationarity, there can indeed be instances (e.g. extreme events such as storms) where the actual observations (to be reconstructed) drift outside the concentration-discharge range spanned by the training data (anchoring observations). Since machine learning approaches can struggle with extrapolation outside the range of training data [Liu et. al. 2021], it is useful to calculate the proportion of actual observations that lie outside the training C-Q range and assess the reconstruction

accuracy on such points to be aware of the potential shortcomings in reconstructions. [Fig. S8] depicts the percentage of test observations that lie outside the concentration-discharge range of training data, for each solute-sampling interval combination during stormflow periods. The following tables indicate the reconstruction accuracy on such points (true observations lying outside training range) for each catchment.

Solute	*Sampling frequency of training data (hours)*						
	4	**8**	**12**	**18**	**24**	**36**	**48**
Ca	0.83	0.70	0.71	0.29	0.50	0.35	0.42
Mg	0.84	0.71	0.27	0.00	0.00	0.00	0.00
Na	**n.a.**	0.97	0.93	0.75	0.74	0.66	0.00
K	0.90	0.84	0.81	0.78	0.77	0.79	0.59
Cl	**n.a.**	0.98	0.96	0.92	0.79	0.63	0.00
SO_4	0.99	0.99	0.95	0.88	0.86	0.68	0.00
NO_3	0.77	0.86	0.79	0.75	0.41	0.03	0.00

Table 2(a): Out-of-distribution reconstruction accuracy (Stormflow: Orgeval)

Solute	*Sampling frequency of training data (hours)*										
	4	**8**	**12**	**18**	**24**	**36**	**48**	**60**	**72**	**96**	**120**
Ca	1	1	0.99	0.94	0.97	0.88	0.89	0.91	0.94	0.58	0.72
Mg	0.98	0.99	0.88	0.99	0.95	0.98	0.95	0.90	0.89	0.84	0.74
Na	**n.a.**	0.86	0.90	0.99	0.88	1	0.83	0.91	0.93	0.78	0.78
K	**n.a.**	0.97	0.71	0.67	0.89	0.60	0.13	0.77	0.76	0.00	0.23
Cl	1	0.97	1	0.98	0.98	0.95	0.93	0.95	0.95	0.84	0.75
SO_4	**n.a.**	0.71	0.62	0.05	0.93	0.91	0.89	0.96	0.91	0.84	0.83
NO_3	0.85	0.78	0.88	0.56	0.79	0.84	0.38	0.89	0.51	0.67	0.94

Table 2(b): Out-of-distribution reconstruction accuracy (Stormflow: Monticello)

Solute	*Sampling frequency of training data (hours)*					
	14	**21**	**35**	**49**	**70**	**84**
Ca	**n.a.**	**n.a.**	**n.a.**	0.93	0.41	0.79
Mg	**n.a.**	**n.a.**	**n.a.**	0.80	0.44	0.67
Na	**n.a.**	**n.a.**	**n.a.**	0.70	0.64	0.74
K	**n.a.**	**n.a.**	0.00	0.30	0.00	0.00
Cl	**n.a.**	**n.a.**	0.61	0.84	0.76	0.72
NO_3	**n.a.**	**n.a.**	0.73	0.76	0.68	0.55
SO_4	**n.a.**	**n.a.**	0.62	0.44	0.21	0.77
Si	**n.a.**	**n.a.**	0.85	0.90	0.59	0.84
Table 2(c): Out-of-distribution reconstruction accuracy (Stormflow: Plynlimon)						

220

Table 2: Reconstruction accuracy on test observations that lie outside the concentration-discharge range spanned by training data, quantified using R^2 values between reconstructed vs. original data. Cells marked 'n.a.' mean very few (<10) observations outside the training range, indicating that training range (almost) covers the whole testing range.

S5. Gap-filling of time series using Singular Spectrum Analysis

While the machine learning framework primarily reconstructs solute concentrations from continuous physico-chemical sensor data, the reliability of these predictions depends on the availability of the predictors themselves. An approach based on Singular Spectrum Analysis (SSA) was implemented here to impute the gaps. The process begins by embedding the time series into a trajectory matrix, using a sliding window over the time series. This matrix is then subjected to Singular Value Decomposition to extract the principal components of this signal. After selecting only those components that represent the signal and discarding those associated with high-frequency noise (analogous to choosing components to retain in PCA, using heuristics such as Kaiser rule [Jackson 1993]), the time series is reconstructed through diagonal averaging. The optimal window length and components for reconstruction were calibrated by tuning on artificially created data gaps. The effectiveness of SSA for gap-filling was evaluated through the following approach. First, artificial gaps of varying lengths were introduced into continuous predictor records. These gaps were then reconstructed using the algorithm, and its performance was compared against commonly used imputation methods (namely, linear interpolation, spline interpolation, nearest-neighbor imputation, ARIMA-based imputation). Accuracy was quantified using R^2 and RMSE values between the actual (artifically masked) observations and the imputed observations. The results are shown in [Fig. S7]

S6. Economic viability of proposed monitoring strategy

The financial barrier to conventional high-frequency monitoring is quantifiable through the lens of analytical throughput and consumable costs. A conservative rate for ion chromatographic analysis of major cations and anions is 10-15 euros per sample, assuming an already equipped laboratory and large batch sizes. Measuring stream chemistry at an hourly resolution results in an annual analytical cost greater than 100,000 euros (n=8700 samples). Conversely, the adoption of the ML-augmented hybrid strategy outlined in this work could massively relieve the financial load. A 24-hour sampling interval could reduce the annual analytical budget to ≈ 4500 euros (n=365), a 95% reduction. This estimate scales linearly with the reduction in sampling effort. This estimate remains conservative, as it excludes significant upfront capital expenditure unique to fully automated high-frequency strategies such as bankside analyzers or lab-in-the-field setups.

Several cost components remain invariant between the two strategies. Both involve initial site characterization, periodic calibration of sensors, quality assurance/quality control protocols and (differing amounts of) laboratory measurements. While the hybrid strategy does not eliminate laboratory dependency, the primary source of cost reduction lies in its substitution of direct chemical analyses with model-inferred estimates at a higher temporal resolution. Ion chromatography, reagent consumption, sample preservation, and associated logistics scale directly with sample number, whereas sensor-based measurements exhibit low marginal costs once deployed. Additionally, the hybrid approach minimizes consumables (e.g., vials, filters, reagents) and reduces wear on analytical instrumentation, indirectly lowering maintenance and replacement costs. Personnel costs, although often treated as secondary, scale (possible non-linearly) with sampling efforts. High-frequency manual or semi-automated strategies require frequent site visits for sample retrieval, instrument maintenance, and troubleshooting. In contrast, the hybrid approach limits physical interventions to low-frequency sampling campaigns and routine sensor maintenance. It is also worth noting that the hardware costs supporting this hybrid strategy are increasingly accessible. Professional-grade, submersible sensors for pH/EC/Temperature range between 500-1000 euros, and the computational costs are negligible since the scripts can be run on any modern-day personal computer.

Beyond financial considerations, the two strategies also diverge significantly in their carbon footprint. Conventional high-frequency sampling entails repeated field visits (vehicular

emissions), energy-intensive laboratory analyses (e.g., ion chromatography systems, sample refrigeration), and consumable production and disposal. Assuming even modest travel requirements, transportation alone can contribute substantially to annual CO_2 emissions. In contrast, the hybrid strategy reduces laboratory throughput by an order of magnitude and shifts the monitoring burden toward low-power in-situ sensors which have comparatively minor electricity usage and associated emissions. While sensor manufacturing and deployment carry an initial carbon cost, these parameters are also monitored alongside most, if not all, traditional high-frequency river chemistry measurement efforts, and thus form a shared baseline environmental cost. Moreover, this is amortized over extended deployment periods and is negligible relative to the cumulative emissions of sustained high-frequency laboratory analysis.

S7. **Softwares and reproducibility**

The analyses presented in this study were conducted under Python version 3.12 on a computer running Ubuntu 24.04.2 LTS. The libraries Numpy v2.3.3, Pandas v2.3.3, Scipy v1.15.3, and Matplotlib v3.10.7 were used for data manipulation, statistical analysis and data visualization. The libraries Scikit-Learn v1.8, LightGBM v4.6, XGBoost v3.0.5, and Optuna v4.8.0 were used for machine learning model development and hyperparameter tuning, and Singular Spectrum Analysis was performed using the library SSALib v0.1.3.

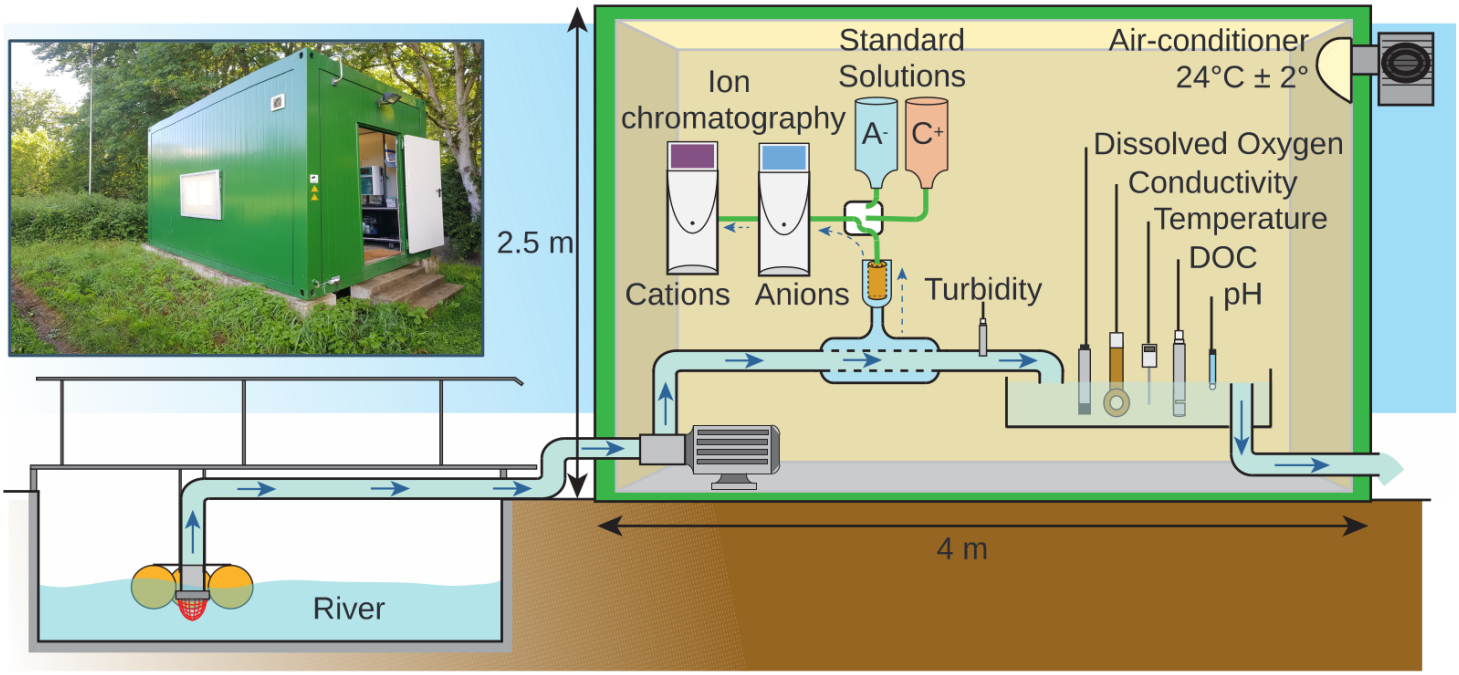

Fig. S1: RiverLab at the Orgeval CZO, France. This is an example of a 'lab-in-the field' setup, used for the acquisition of high-frequency major solute measurements. Stream water is continously sampled from the stream, and is routed towards a series of probes for the measurement of Dissolved O_2, Electrical conductivity, Temperature, pH, Turbidity and Dissolved Organic Carbon. A portion of this sampled water undergoes filtration and is measured for major cations and anions through two ion chromatographs located on-site. Figure modified after [Floury et. al. 2017]

Fig. S2: First-order summary of the SHAP analyses presented in figures S3–S6, shown for the top 5 predictors across all catchment-period-target combinations. Green background indicates that an increase in the predictor value (on an average) increases the solute concentrations, and brown background indicates that an increase in predictor leads to decreased solute concentrations. Pink backgrounds imply a highly non-linear relationship that could not be summarized using a simple increase/decrease relationship. Higher values indicate a stronger magnitude of influence of the predictor on solute concentrations (for the corresponding catchment-period combination)

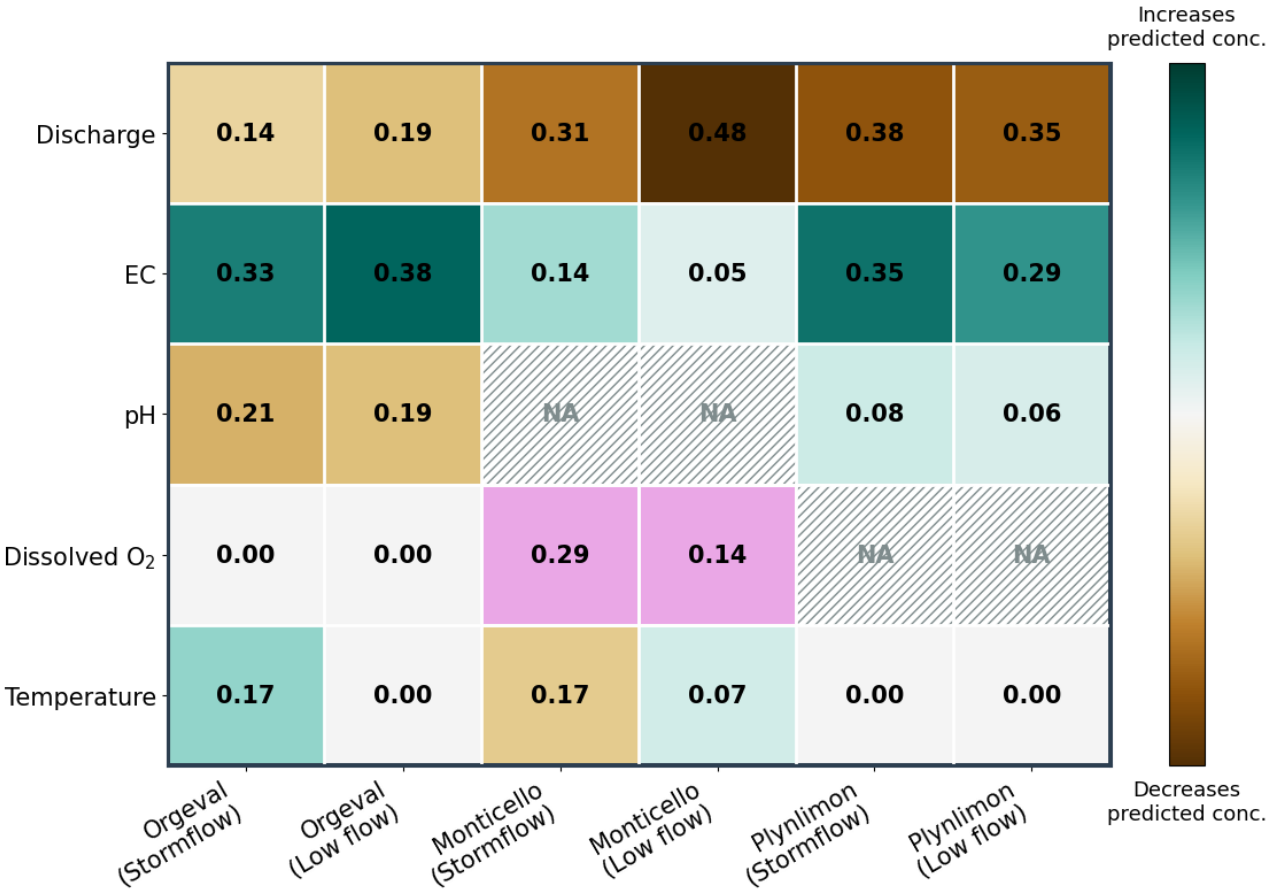

Fig. S3-S6 are presented respectively, in the following three pages.

Fig. S3: SHAP beeswarm plots, for target solute-hydrological period combinations in the **Orgeval** catchment. The predictors are ranked by their relative importance in influencing the target solute predictions. The figure describes the magnitude and direction of a predictor's impact on the prediction. The x-axis units are the same as the target solute concentration units. Each point in a figure corresponds to a specific observation, and the color represents the predictor's value at that point relative to its overall range.

Fig. S4: SHAP plots for the Monticello catchment.

Fig. S5: SHAP plots for the Plynlimon catchment.

Glossary for predictor names used in Fig. S3-S5:

- **Q:** River discharge
- **O_2:** Dissolved oxygen
- **Cond or EC:** Electrical Conductivity
  - **EC_24h** denotes the rolling mean of 24-hour antecedent conductivity
- **limb_type**: Ascending/descending limb of a storm event, encoded in a binary value.
- **slope_rel:** Local slope of the hydrograph (dQ/dt)

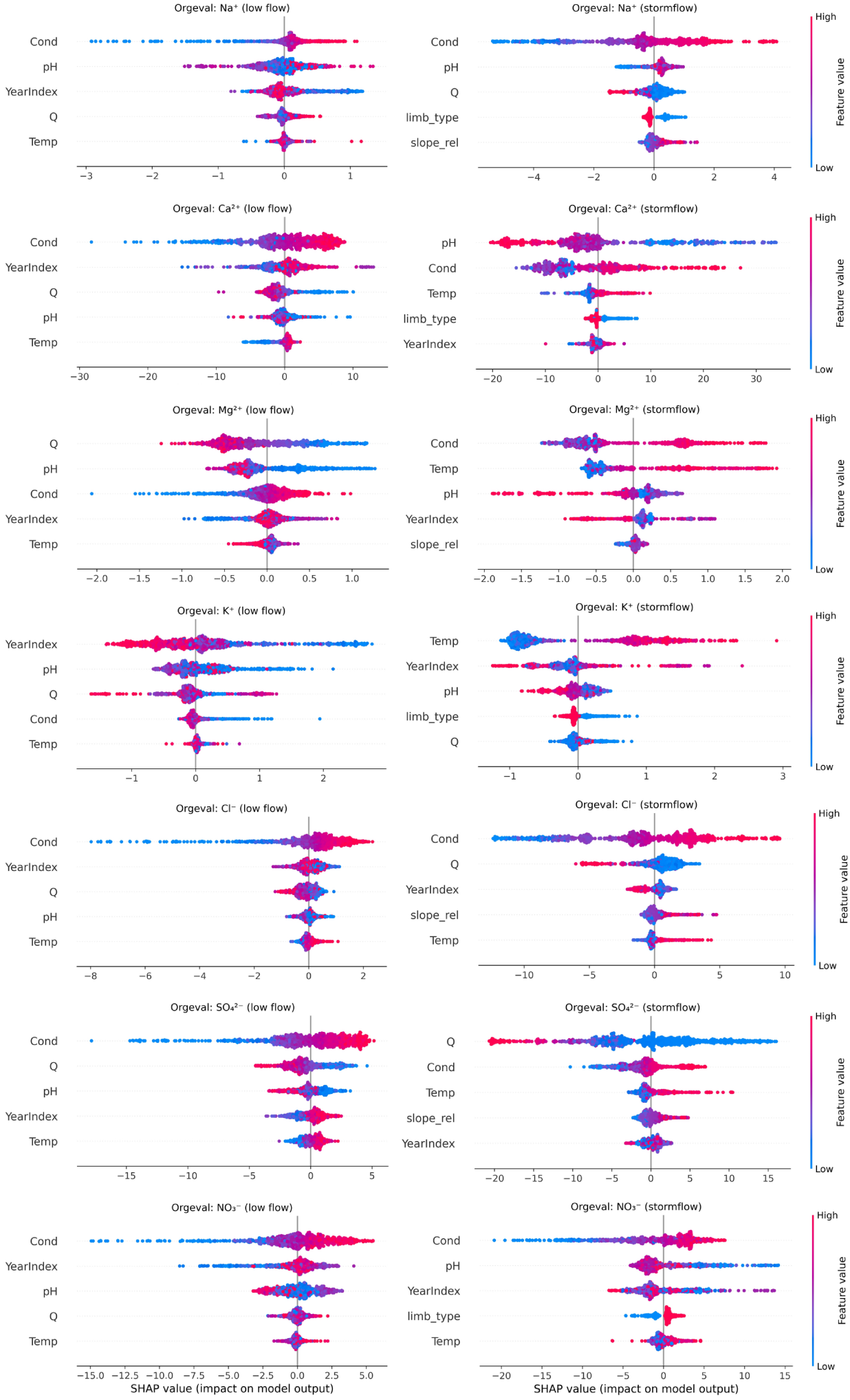
Orgeval: Na⁺ (low flow)
Cond
pH
YearIndex
Q
Temp
−3 −2 −1 0 1
Orgeval: Na⁺ (stormflow)
Cond
pH
Q
limb_type
slope_rel
−4 −2 0 2 4
Orgeval: Ca²⁺ (low flow)
Cond
YearIndex
Q
pH
Temp
−30 −20 −10 0 10
Orgeval: Ca²⁺ (stormflow)
pH
Cond
Temp
limb_type
YearIndex
−20 −10 0 10 20 30
Orgeval: Mg²⁺ (low flow)
Q
pH
Cond
YearIndex
Temp
−2.0 −1.5 −1.0 −0.5 0.0 0.5 1.0
Orgeval: Mg²⁺ (stormflow)
Cond
Temp
pH
YearIndex
slope_rel
−2.0 −1.5 −1.0 −0.5 0.0 0.5 1.0 1.5 2.0
Orgeval: K⁺ (low flow)
YearIndex
pH
Q
Cond
Temp
−1 0 1 2
Orgeval: K⁺ (stormflow)
Temp
YearIndex
pH
limb_type
Q
−1 0 1 2 3
Orgeval: Cl⁻ (low flow)
Cond
YearIndex
Q
pH
Temp
−8 −6 −4 −2 0 2
Orgeval: Cl⁻ (stormflow)
Cond
Q
YearIndex
slope_rel
Temp
−10 −5 0 5 10
Orgeval: SO₄²⁻ (low flow)
Cond
Q
pH
YearIndex
Temp
−15 −10 −5 0 5
Orgeval: SO₄²⁻ (stormflow)
Q
Cond
Temp
slope_rel
YearIndex
−20 −15 −10 −5 0 5 10 15
Orgeval: NO₃⁻ (low flow)
Cond
YearIndex
pH
Q
Temp
−15.0 −12.5 −10.0 −7.5 −5.0 −2.5 0.0 2.5 5.0
SHAP value (impact on model output)
Orgeval: NO₃⁻ (stormflow)
Cond
pH
YearIndex
limb_type
Temp
−20 −15 −10 −5 0 5 10 15
SHAP value (impact on model output)
High
Feature value
Low

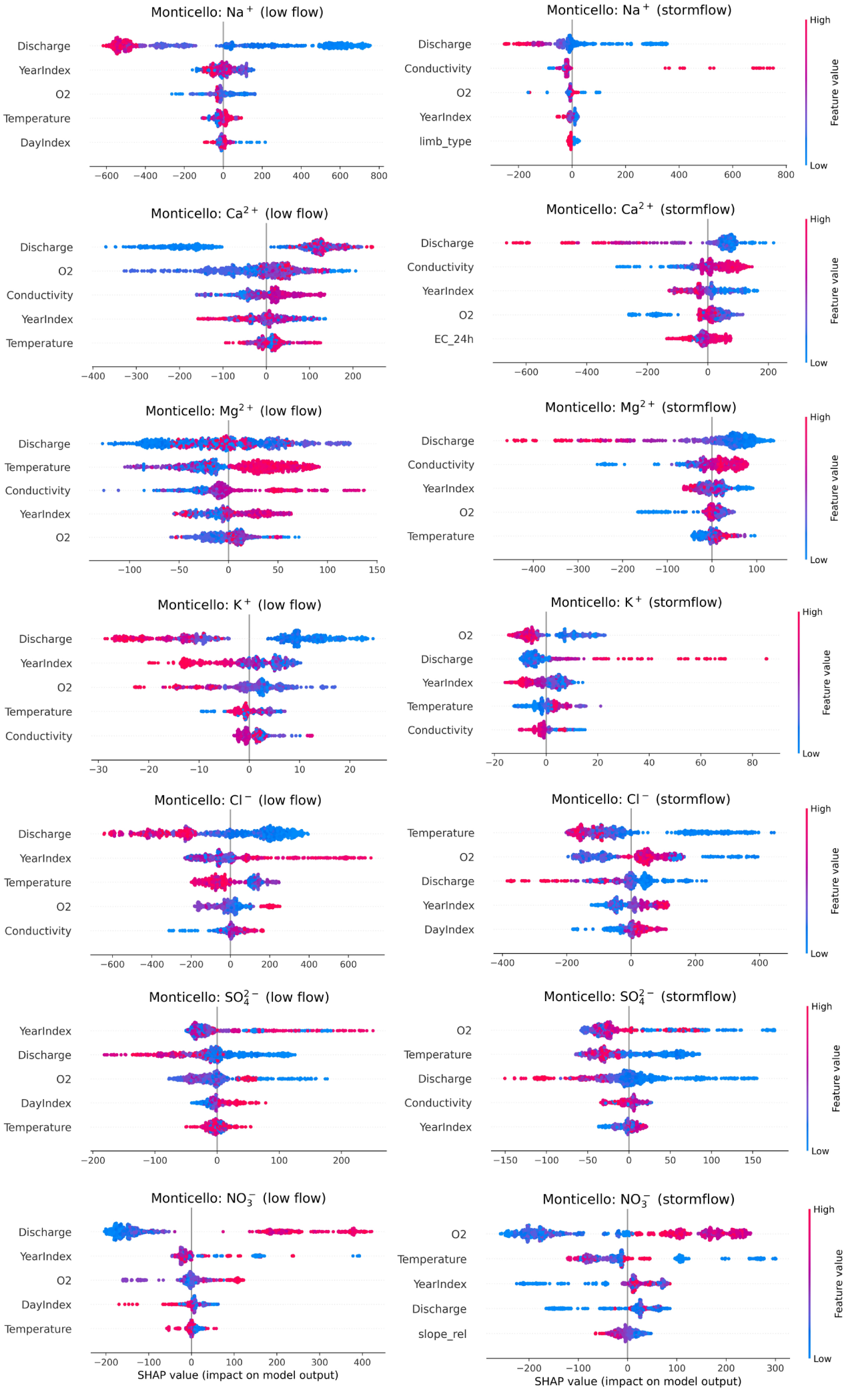
Monticello: Na^+ (low flow)
Discharge
YearIndex
O2
Temperature
DayIndex
−600 −400 −200 0 200 400 600 800
Monticello: Na^+ (stormflow)
Discharge
Conductivity
O2
YearIndex
limb_type
−200 0 200 400 600 800
High
Feature value
Low
Monticello: Ca^{2+} (low flow)
Discharge
O2
Conductivity
YearIndex
Temperature
−400 −300 −200 −100 0 100 200
Monticello: Ca^{2+} (stormflow)
Discharge
Conductivity
YearIndex
O2
EC_24h
−600 −400 −200 0 200
High
Feature value
Low
Monticello: Mg^{2+} (low flow)
Discharge
Temperature
Conductivity
YearIndex
O2
−100 −50 0 50 100 150
Monticello: Mg^{2+} (stormflow)
Discharge
Conductivity
YearIndex
O2
Temperature
−400 −300 −200 −100 0 100
High
Feature value
Low
Monticello: K^+ (low flow)
Discharge
YearIndex
O2
Temperature
Conductivity
−30 −20 −10 0 10 20
Monticello: K^+ (stormflow)
O2
Discharge
YearIndex
Temperature
Conductivity
−20 0 20 40 60 80
High
Feature value
Low
Monticello: Cl^- (low flow)
Discharge
YearIndex
Temperature
O2
Conductivity
−600 −400 −200 0 200 400 600
Monticello: Cl^- (stormflow)
Temperature
O2
Discharge
YearIndex
DayIndex
−400 −200 0 200 400
High
Feature value
Low
Monticello: SO_4^{2-} (low flow)
YearIndex
Discharge
O2
DayIndex
Temperature
−200 −100 0 100 200
Monticello: SO_4^{2-} (stormflow)
O2
Temperature
Discharge
Conductivity
YearIndex
−150 −100 −50 0 50 100 150
High
Feature value
Low
Monticello: NO_3^- (low flow)
Discharge
YearIndex
O2
DayIndex
Temperature
−200 −100 0 100 200 300 400
SHAP value (impact on model output)
Monticello: NO_3^- (stormflow)
O2
Temperature
YearIndex
Discharge
slope_rel
−200 −100 0 100 200 300
SHAP value (impact on model output)
High
Feature value
Low

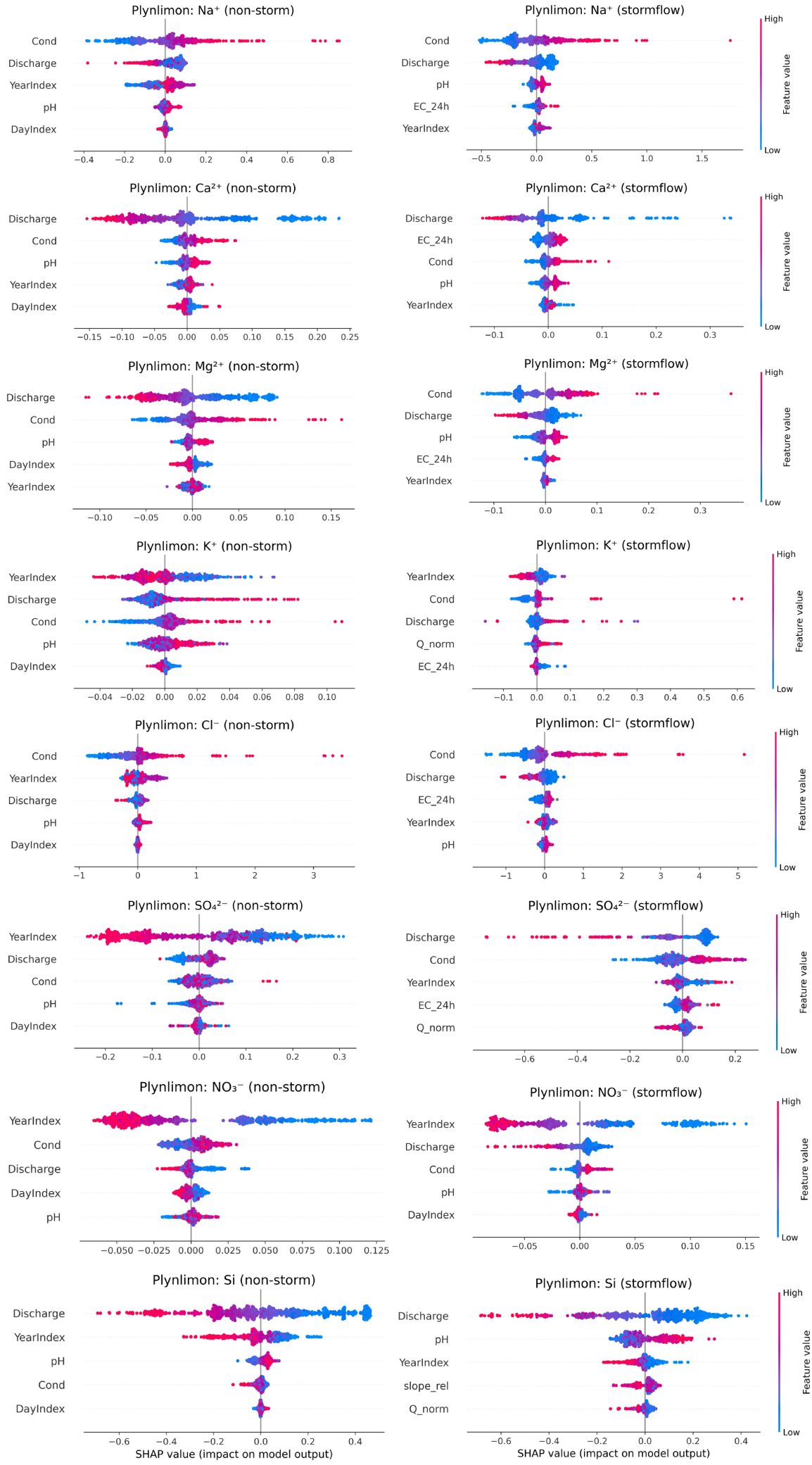
Plynlimon: Na⁺ (non-storm)
Cond
Discharge
YearIndex
pH
DayIndex
−0.4 −0.2 0.0 0.2 0.4 0.6 0.8
Plynlimon: Na⁺ (stormflow)
Cond
Discharge
pH
EC_24h
YearIndex
−0.5 0.0 0.5 1.0 1.5
High
Feature value
Low
Plynlimon: Ca²⁺ (non-storm)
Discharge
Cond
pH
YearIndex
DayIndex
−0.15 −0.10 −0.05 0.00 0.05 0.10 0.15 0.20 0.25
Plynlimon: Ca²⁺ (stormflow)
Discharge
EC_24h
Cond
pH
YearIndex
−0.1 0.0 0.1 0.2 0.3
High
Feature value
Low
Plynlimon: Mg²⁺ (non-storm)
Discharge
Cond
pH
DayIndex
YearIndex
−0.10 −0.05 0.00 0.05 0.10 0.15
Plynlimon: Mg²⁺ (stormflow)
Cond
Discharge
pH
EC_24h
YearIndex
−0.1 0.0 0.1 0.2 0.3
High
Feature value
Low
Plynlimon: K⁺ (non-storm)
YearIndex
Discharge
Cond
pH
DayIndex
−0.04 −0.02 0.00 0.02 0.04 0.06 0.08 0.10
Plynlimon: K⁺ (stormflow)
YearIndex
Cond
Discharge
Q_norm
EC_24h
−0.1 0.0 0.1 0.2 0.3 0.4 0.5 0.6
High
Feature value
Low
Plynlimon: Cl⁻ (non-storm)
Cond
YearIndex
Discharge
pH
DayIndex
−1 0 1 2 3
Plynlimon: Cl⁻ (stormflow)
Cond
Discharge
EC_24h
YearIndex
pH
−1 0 1 2 3 4 5
High
Feature value
Low
Plynlimon: SO₄²⁻ (non-storm)
YearIndex
Discharge
Cond
pH
DayIndex
−0.2 −0.1 0.0 0.1 0.2 0.3
Plynlimon: SO₄²⁻ (stormflow)
Discharge
Cond
YearIndex
EC_24h
Q_norm
−0.6 −0.4 −0.2 0.0 0.2
High
Feature value
Low
Plynlimon: NO₃⁻ (non-storm)
YearIndex
Cond
Discharge
DayIndex
pH
−0.050 −0.025 0.000 0.025 0.050 0.075 0.100 0.125
Plynlimon: NO₃⁻ (stormflow)
YearIndex
Discharge
Cond
pH
DayIndex
−0.05 0.00 0.05 0.10 0.15
High
Feature value
Low
Plynlimon: Si (non-storm)
Discharge
YearIndex
pH
Cond
DayIndex
−0.6 −0.4 −0.2 0.0 0.2 0.4
SHAP value (impact on model output)
Plynlimon: Si (stormflow)
Discharge
pH
YearIndex
slope_rel
Q_norm
−0.6 −0.4 −0.2 0.0 0.2 0.4
SHAP value (impact on model output)
High
Feature value
Low

Fig. S6: Reconstruction accuracy of high-frequency solute concentrations against varying intervals of low-frequency 'anchoring' observations used to train the model. Blue and green dashed lines denote reconstruction performance for stormflow and low-flow periods respectively, and thick red line represents all periods (including transitionary flow) pooled together. Accuracy is quantified using Nash–Sutcliffe Efficiency, with values greater than 0.75 (depicted via horizontal grey line) considered a threshold for optimal predictions. Yellow and checkered red background shading indicate severity of insufficiency in training data, leading to degraded model predictions.

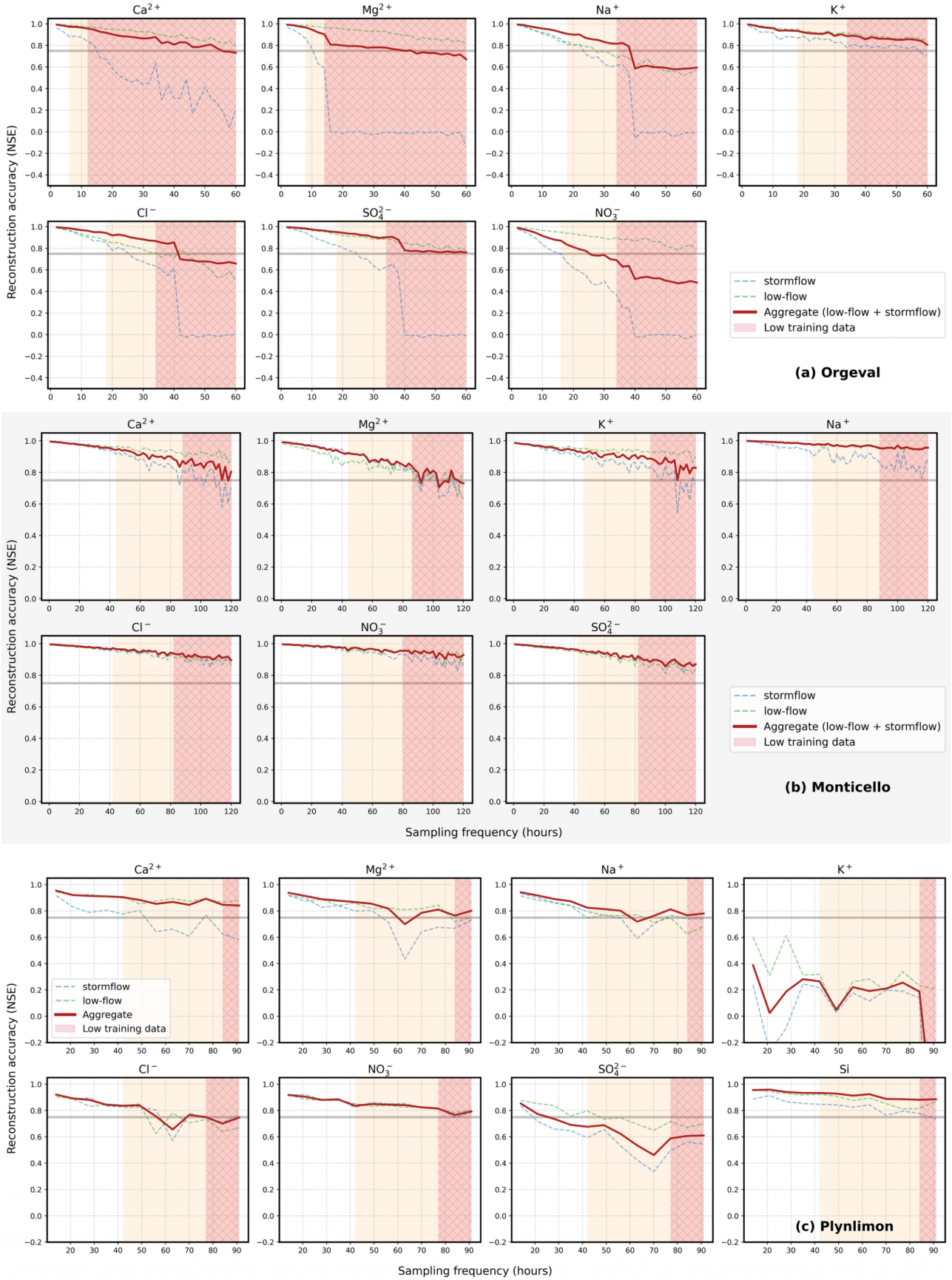

Fig. S7: (a) Comparison of linear interpolation and SSA-based imputation approach, illustrated using artifically masked gaps in water temperature time series measured at Orgeval catchment. SSA-based reconstruction preserves the high-frequency variations which is muted in linear interpolation-based gap filling. **(b)** Comparison of SSA-based imputation against commonly used gap-filling techniques, quantified using R^2 & root mean square error (RMSE) values between original values and imputed values.

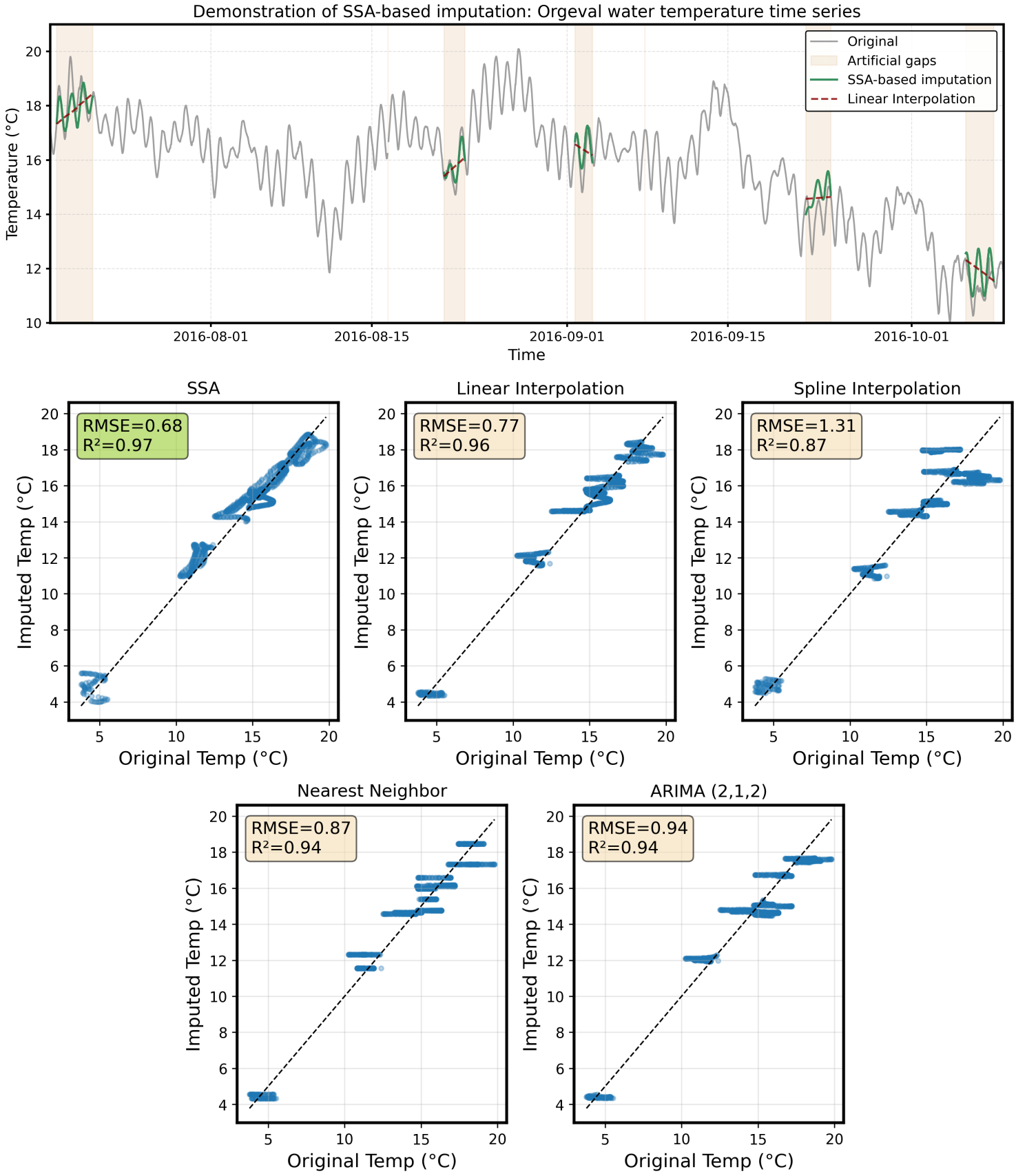

Fig. S8: Percentage of test observations that lie outside the concentration–discharge range of training data, for each solute–sampling interval combination.

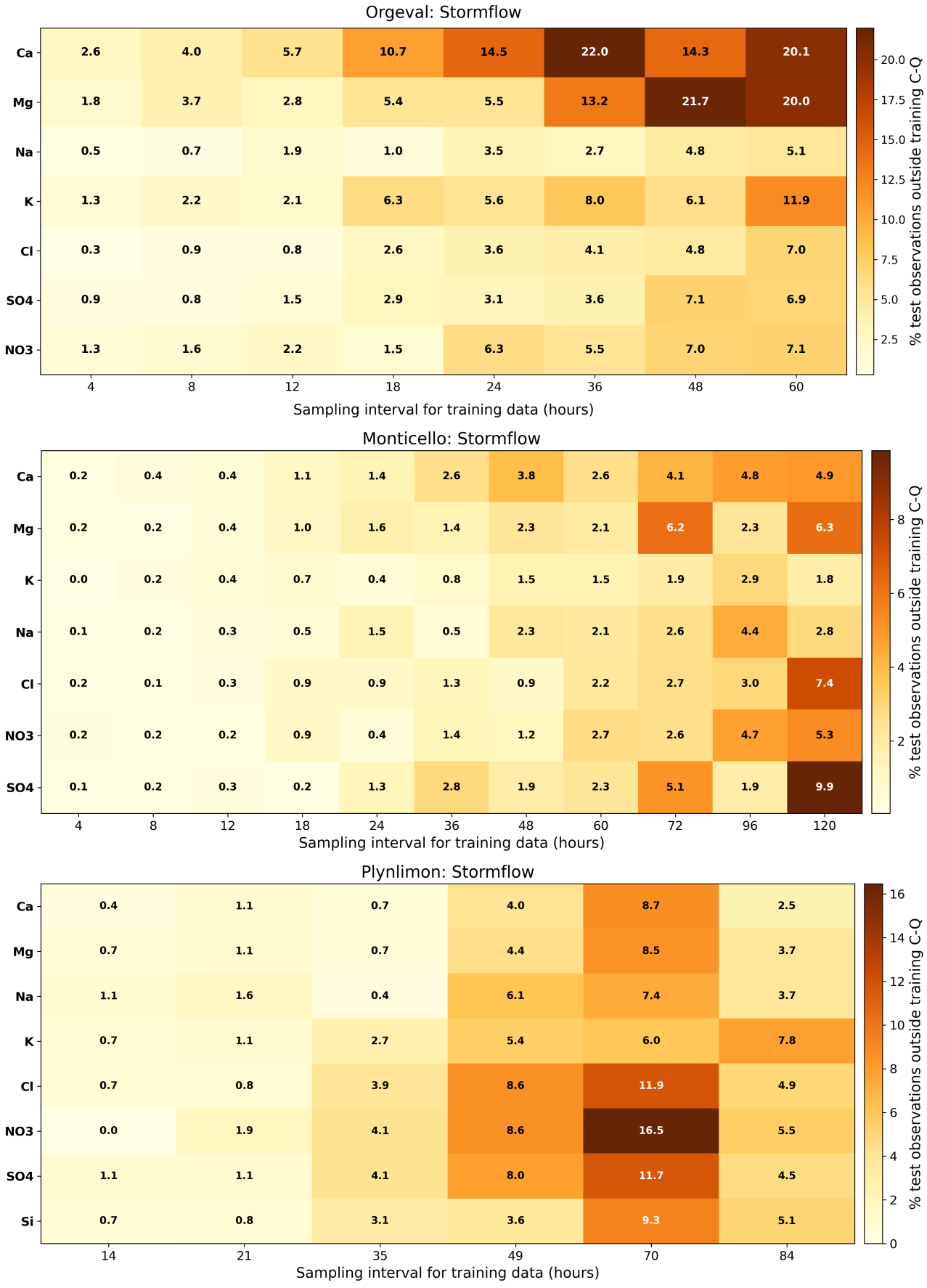

370

Fig. S9 Delineation of the data into hydrological regimes based on discharge – an example from Orgeval catchment.

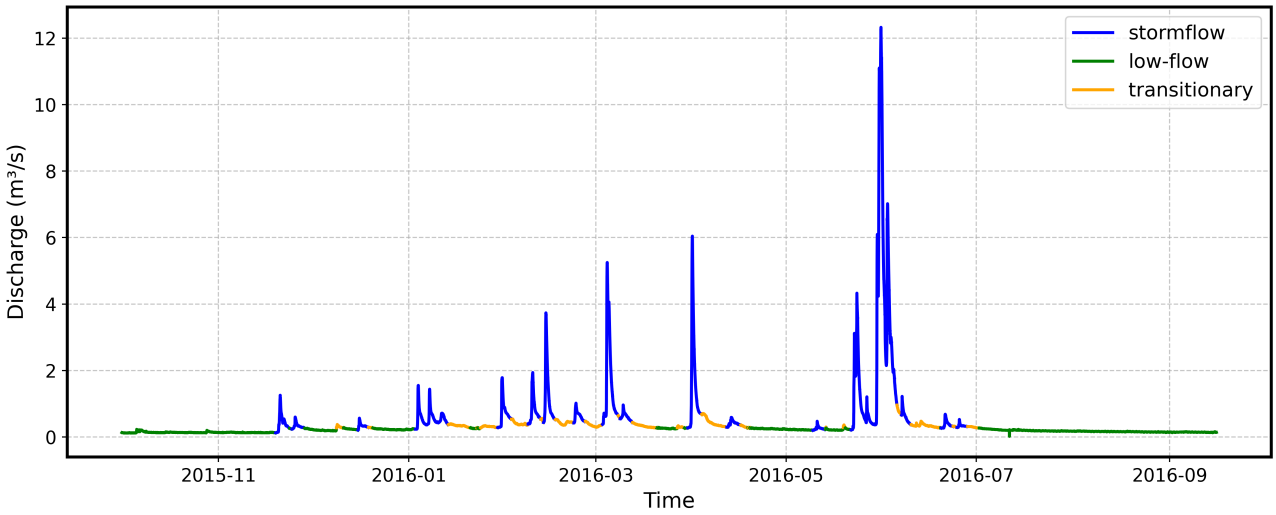

References

Akiba, T., Sano, S., Yanase, T., Ohta, T., & Koyama, M. (2019). Optuna: A Next-generation Hyperparameter Optimization Framework. Proceedings of the 25th ACM SIGKDD International Conference on Knowledge Discovery & Data Mining, 2623–2631. https://doi.org/10.1145/3292500.3330701

Ansart, P., Azougui, A., Blanchouin, A., Cordier, L., Floury, P., Gaillardet, J., Nespoulet, R., & Tallec, G. (2020). High-frequency acquisition of stream chemical data on ORACLE observatory [Dataset]. Recherche Data Gouv. https://doi.org/10.15454/9PUYPN

Floury, P., Gaillardet, J., Gayer, E., Bouchez, J., Tallec, G., Ansart, P., Koch, F., Gorge, C., Blanchouin, A., & Roubaty, J.-L. (2017). The potamochemical symphony: New progress in the high-frequency acquisition of stream chemical data. Hydrology and Earth System Sciences, 21(12), 6153–6165. https://doi.org/10.5194/hess-21-6153-2017

Jackson, D. A. (1993). Stopping Rules in Principal Components Analysis: A Comparison of Heuristical and Statistical Approaches. Ecology, 74(8), 2204–2214. https://doi.org/10.2307/1939574

Knapp, J. L. A., Von Freyberg, J., Studer, B., Kiewiet, L., & Kirchner, J. W. (2020). Concentration–discharge relationships vary among hydrological events, reflecting differences in event characteristics. Hydrology and Earth System Sciences, 24(5), 2561–2576. https://doi.org/10.5194/hess-24-2561-2020

Liu, J., Shen, Z., He, Y., Zhang, X., Xu, R., Yu, H., & Cui, P. (2021). Towards Out-Of-Distribution Generalization: A Survey (Version 2). arXiv. https://doi.org/10.48550/ARXIV.2108.13624

Neal, C., Reynolds, B., Kirchner, J. W., Rowland, P., Norris, D., Sleep, D., Lawlor, A., Woods, C., Thacker, S., Guyatt, H., Vincent, C., Lehto, K., Grant, S., Williams, J., Neal, M., Wickham, H., Harman, S., & Armstrong, L. (2013). High-frequency precipitation and stream water quality time series from Plynlimon, Wales: An openly accessible data resource spanning the periodic table. Hydrological Processes, 27(17), 2531–2539. https://doi.org/10.1002/hyp.9814

Wang, J., Bouchez, J., Winnick, M. J., Goodwell, A. E., Dere, A., Kumar, P., & Druhan, J. L. (2025). Drought constrictions on lateral carbon transport. Nature Geoscience, 18(11), 1138–1143. https://doi.org/10.1038/s41561-025-01807-z